Nesting of thermodynamic, structural, and dynamic anomalies in liquid silicon

Vishwas V. Vasisht, John Mathew, Shiladitya Sengupta, and Srikanth Sastry

Citation: The Journal of Chemical Physics **141**, 124501 (2014); doi: 10.1063/1.4880559
View online: http://dx.doi.org/10.1063/1.4880559
View Table of Contents: http://scitation.aip.org/content/aip/journal/jcp/141/12?ver=pdfcov
Published by the AIP Publishing

Nesting of thermodynamic, structural, and dynamic anomalies in liquid silicon

Vishwas V. Vasisht,[1,a)] John Mathew,[2] Shiladitya Sengupta,[3,b)] and Srikanth Sastry[1,3]
[1]*Theoretical Sciences Unit, Jawaharlal Nehru Centre for Advanced Scientific Research, Jakkur Campus, Bengaluru 560 064, India*
[2]*Department of Condensed Matter Physics and Materials Science, Tata Institute of Fundamental Research, Homi Bhabha Road, Mumbai 400 005, India*
[3]*TIFR Centre for Interdisciplinary Sciences 21, Brundavan Colony, Narsingi, Hyderabad 500075, India*

(Received 24 March 2014; accepted 19 May 2014; published online 22 September 2014)

Anomalous behaviour in density, diffusivity, and structural order is investigated for silicon modeled by the Stillinger-Weber potential by performing molecular dynamics simulations. As previously reported in the case of water [J. R. Errington and P. G. Debenedetti, Nature (London) **409**, 318 (2001)] and silica [M. S. Shell, P. G. Debenedetti, and A. Z. Panagiotopoulos, Phys. Rev. E **66**, 011202 (2002)], a cascading of thermodynamic, dynamic, and structural anomalous regions is also observed in liquid silicon. The region of structural anomaly includes the region of diffusivity anomaly, which in turn encompasses the region of density anomaly (which is unlike water but similar to silica). In the region of structural anomaly, a tight correlation between the translational and tetrahedrality order parameter is found, but the correlation is weaker when a local orientational order parameter (q_3) is used as a measure of tetrahedrality. The total excess entropy and the pair correlation entropy are computed across the phase diagram and the correlation between the excess entropy and the regions of anomalies in the phase diagram of liquid silicon is examined. Scaling relations associating the excess entropy with the diffusion coefficient show considerable deviation from the quasi-universal behaviour observed in hard-sphere and Lennard-Jones liquids and some liquid metals. Excess entropy based criteria for diffusivity and structural anomalies fail to capture the observed regions of anomaly. © *2014 AIP Publishing LLC*. [http://dx.doi.org/10.1063/1.4880559]

I. INTRODUCTION

In liquid water, below $T = 4\,^{\circ}\mathrm{C}$ at normal pressure, the density decreases with a decrease in temperature, and this behaviour is termed as anomalous—a behaviour which is opposite of what is commonly observed (density monotonically increases with decrease in temperature). This feature in water is the most well known anomaly among many anomalies which have been studied for over a century.[1] Water also exhibits anomalous behaviour in thermodynamic response functions, the compressibility, and heat capacity. The compressibility of water decreases with a decrease in temperature, but reaches a minimum at 46 °C and below this temperature the compressibility increases with a decrease in temperature. Similarly, the specific heat capacity of liquid water decreases with a decrease in temperature but passes through a minimum at 36 °C showing an anomalous increase at lower temperatures. To understand these thermodynamic anomalies in water various models and scenarios have been put forth,[2–8] some of which are based on thermodynamic constraints and novel phase behaviour. Along with the thermodynamic anomalies dynamical anomalies have been also observed.[9] It has been observed below a certain temperature that the diffusivity of liquid water (along an isotherm) increases with increase in pressure (or density)[9] and this feature is termed as the diffusivity anomaly. These anomalies in thermodynamic and dynamical properties, which are often termed as water-like anomalies, have been also found in various model potentials and materials including silica[10] and silicon.[12,13]

In order to understand the microscopic origins of the water-like anomalies, in recent years, many computer simulation studies (on different materials and model potentials) have carefully looked at the relationship between the above stated anomalies and structural ordering[9,10,14–17] as well as the nature of molecular interactions.[18–27] In liquid water and other liquids which exhibit orientation dependent interaction and have locally ordered structures, the molecules (or atoms) form an energetically stable tetrahedral open structure. To understand the dependence of anomalies in thermodynamics and dynamics on underlying structural properties, one needs to carefully quantify the structural ordering in a liquid. In one of first studies along these lines, Errington and Debenedetti[9] analysed the local structural ordering, in the SPC/E model of water, using a translational order parameter (t_{trans}) and a tetrahedrality order parameter (q_{tetra}) and found that the q_{tetra} distribution (at a fixed density) is bimodal. This feature in the distribution was found to be not due to the existence of two fixed types of energetically favoured arrangements, but due to the presence of a transient arrangement of tetrahedrally coordinated molecules and distorted or non-tetrahedral molecules. Further, using these order parameters, the authors identified a structurally anomalous region in the phase diagram

[a)]Present address: Institute for Building Materials, ETH, 8093 ETH, Zurich, Switzerland.
[b)]Present address: The Department of Chemical Physics, The Weizmann Institute of Science, Rehovot 76100, Israel.

(defined, along an isotherm, by a tetrahedrality order parameter maximum at low densities and translational order parameter minimum at high densities). In this structurally anomalous region the two structural orders were found to be strictly correlated (for a particular value of q_{tetra} a unique value of t_{trans} is associated). The loci of structural order extrema (in the (T − ρ) plane of phase diagram) were found to enclose the region of anomalous diffusion (demarcated by the loci of diffusivity extrema), which was found in turn to enclose the region of density anomaly, suggesting the influence of structural order on the liquid anomalies. A similar analysis was carried out by Shell *et al.*[10] for silica (using the van Beest, Kramer, and van Santen (BKS) model potential) and the authors found that even though most of the features were akin to that of the water, there were two exceptions. In the structurally anomalous region, unlike in water, the structural order parameters were not perfectly correlated (hypothesised to be due to the model interaction potential which gives broader extrema in the structural order parameters) and second the loci of diffusivity extrema enclosed the structural and thermodynamic anomaly regions. Based on these observations the authors concluded that structural order parameters used in the analysis do not anticipate the occurrence of the diffusivity anomaly and hence do not provide a satisfactory microscopic picture of the anomalous behaviour in silica.[10] Recently, similar studies have been carried out exploring the structural origins behind the various anomalies in different model potentials of water, ionic liquids, and liquids characterised by the Stillinger-Weber potential, including silicon.[24,25] These works suggest that a strong correlation between the density anomaly and tetrahedral ordering exists only in rigid-body model potentials for water and Stillinger-Weber liquids (in a limited range of tetrahedrality strength), but not in ionic melts. The water-like cascading of anomalous regions in the phase diagram has been observed not only in systems having directional interactions but also in the simulation studies of spherically symmetric potentials[18,20,21,28] (and references within). These studies[18] suggest a relation between length scales associated with the interaction potential and water-like anomalies. A recent study of a core-softened model[17] shows that the order of the cascading regions of anomaly can be changed by increasing the depth of the attractive part of the potential.

To obtain a more general picture of the origins of these anomalies, Errington *et al.*[28] attempted to understand these anomalies in terms of the excess entropy. These authors derived various criteria based on excess entropy for observing these anomalies (which we discuss briefly in this paper, before presenting our results). This approach has been tested in various systems[15,16,23,26,27,29,30] and has been able to predict the regions of anomalies in the phase diagram.

In this paper, we present an elaborate analysis of liquid and supercooled liquid silicon, which includes the computation of structural order parameters and excess entropy. We have performed molecular dynamics (MD) simulations using the Stillinger-Weber (SW) potential[31] to investigate the anomalous properties of liquid and supercooled liquid silicon. In a recent review, an extensive comparison with experimental and *ab initio* data showed that the SW potential indeed captures structural and dynamics properties very well and that the deviations from the experimental values are comparable to the spread between different experimental results, and that these differences are comparable to those displayed by *ab initio* results.[32] Using the SW potential, the phase diagram of supercooled liquid silicon has been charted out[13] which includes the liquid-liquid phase coexistence line, liquid-liquid critical point, density extrema, compressibility extrema, and the liquid spinodal, which does not intersect the line of density maxima (which is quite similar to supercooled water[6,33] and silica[34]). Using this phase diagram as a guide, we have computed diffusivity, structural order parameter, and excess entropy in a wide range of state points. Our results show that liquid silicon indeed has a nesting of anomalous regions in the phase diagram. We compute the per-particle excess entropy (s_E) from thermodynamic integration and compare with the per particle two-body excess entropy (s_2) obtained from the pair-correlation function. We have tested the scaling relations that connect the excess entropy with the diffusion coefficient and also verify the relation between the excess entropy and the thermodynamics, dynamic, and structural anomalies.

This paper is organised into four sections. In Sec. II, we discuss details of interaction potential for silicon and methods used to compute various quantities mentioned above. In Sec. III we present our results and we conclude in Sec. IV with a brief discussion and summary.

II. COMPUTATIONAL DETAILS

The Stillinger-Weber potential for silicon comprises of a two- and a three-body interaction potential and is defined as

$$u_{SW} = \sum_{i<j} v_2(r_{ij}/\sigma) + \sum_{i<j<k} v_3(\mathbf{r}_i/\sigma, \mathbf{r}_j/\sigma, \mathbf{r}_k/\sigma), \quad (1)$$

where σ is the diameter of the atoms, $\mathbf{r}_i$ is the position of atom i, and r_{ij} is the distance between atoms i and j. The two-body potential is short-ranged and has the form

$$v_2(r) = \begin{cases} A\epsilon(Br^{-4} - 1)\exp\left(\frac{1}{r-a}\right) & r < a \\ 0 & r \geq a \end{cases}, \quad (2)$$

where $A = 7.049556277$, $B = 0.6022245584$, and $a = 1.8$. The repulsive three-body potential is also short-ranged, and is given by

$$v_3(\mathbf{r}_i, \mathbf{r}_j, \mathbf{r}_k) \equiv h(r_{ij}, r_{ik}, \theta_{jik}) + h(r_{ij}, r_{jk}, \theta_{ijk}) + h(r_{ik}, r_{jk}, \theta_{ikj}), \quad (3)$$

where θ_{jik} is the angle formed by the vectors $\mathbf{r}_{ij}$ and $\mathbf{r}_{ik}$ and

$$h(r_{ij}, r_{ik}, \theta_{jik}) = \epsilon\lambda \exp\left[\frac{\gamma}{r_{ij} - a} + \frac{\gamma}{r_{ik} - a}\right](\cos\theta_{jik} + \alpha)^2 \times H(a - r_{ij})H(a - r_{ik}), \quad (4)$$

where $\lambda = 21.0$, $\gamma = 1.20$, and $H(x)$ is the Heaviside step function. The choice $\alpha = 1/3$ in $(\cos\theta_{jik} + \alpha)^2$ favours a tetrahedral arrangement of atoms as in silicon. The length and energy scales are set by the choice $\sigma = 2.0951$ Å, $\epsilon = 50$ kcal/mol. The strength of the three body potential is determined by the value of λ. The two body part of the potential smoothly goes to zero at the cut off a.

In this work we report properties of liquid and supercooled silicon over a temperature ranging between $T = 1070\,\mathrm{K}$ and $T = 6293\,\mathrm{K}$ and pressure range varying between $P = -3.7\,\mathrm{GPa}$ and $P = 15.0\,\mathrm{GPa}$. The system size we have considered is 512 atoms and the time step is 0.383 fs for all our MD simulations. The equilibration of the system was monitored by calculating the relaxation of intermediate scattering function. At each of the state points we have performed MD simulations for a minimum of ten relaxation times and computed the diffusion coefficient, the structural order parameters, and the excess entropy, which we explain below.

A. Diffusivity

We calculate the self diffusion coefficient D from the slope of mean square displacement in the diffusion regime using the Einstein-Smoluchowski equation given by (for the case of three dimensional system)

$$D = \lim_{t\to\infty} \frac{1}{6t} \langle |\vec{r}(t) - \vec{r}(0)|^2 \rangle. \tag{5}$$

B. Structural order parameters

1. Translational order

The translational order parameter[35] t_{trans} is defined as

$$t_{\mathrm{trans}} = \frac{\int_0^{\xi_c} |g(\xi) - 1| d\xi}{\xi_c}, \tag{6}$$

where $\xi = r\rho^{(1/3)}$ is the scaled coordinate, r is the distance between two atoms, ρ is the number density, and ξ_c is a cutoff distance beyond which the system's radial distribution function cannot be distinguished from its asymptotic value of 1. In all our calculations, ξ_c is chosen to be $4.0\,\sigma$ or 8.38 Å. Scaled coordinates are used so that the above integral sums over an equivalent number of coordinate shells at each density.[35] For an ideal gas, since $g(r) = 1.0$, t_{trans} is zero and for a crystal (which has long range crystalline order) t_{trans} has a finite value depending on the cutoff distance (at cutoff $\xi_c = 4.0\,\sigma$ the crystalline translational order parameter is around 0.6). In the liquid phase t_{trans} will have a value in between that of the ideal gas and a crystal. The numerical integration is carried out using the Simpson's 3/8th rule.

2. Tetrahedrality order

The tetrahedrality order parameter[9] q_{tetra} is defined as

$$q_{\mathrm{tetra}} = 1 - \frac{3}{8} \sum_{j=1}^{3} \sum_{k=j+1}^{4} \left(\cos(\psi_{jk}) + \frac{1}{3} \right)^2, \tag{7}$$

where ψ_{jk} is the angle formed by the lines joining a reference atom i and its nearest neighbours j and k. The average q_{tetra} varies between 0 (in the case of an ideal gas) and 1 (in the case of a cubic diamond crystal).

3. Bond orientational order

The bond orientational order parameter[36] q_l is defined using the spherical harmonics evaluated from the knowledge of unit vectors to the neighbouring atoms. Two atoms are considered to be neighbours if they are within a cutoff distance corresponding to the first minimum of $g(r)$ (≈2.93 Å). If an atom i has atom j as its neighbour at a distance $|\vec{r}_{ij}|$ and with an orientation $\hat{r}_{ij}$, then the bond orientational order parameter for atom i is given by

$$q_{\mathrm{lm}}(i) \equiv \frac{1}{N_n(i)} \sum_{j=1}^{N_n(i)} Y_{lm}(\hat{r}_{ij}), \tag{8}$$

where $N_n(i)$ is the total number of neighbours of atom i, $Y_{lm}(\hat{r}_{ij}) \equiv Y_{\mathrm{lm}}(\theta_{ij}, \phi_{ij})$ are the spherical harmonics calculated along the vector $\hat{r}_{ij}$ between the particles i and j, θ_{ij} and ϕ_{ij} represent the polar and azimuthal angles, respectively. A rotationally invariant local orientational order $q_l(i)$ is defined as

$$q_l(i) = \left(\frac{4\pi}{2l+1} \sum_{m=-l}^{l} |q_{lm}(i)|^2 \right)^{(1/2)}. \tag{9}$$

In case of silicon, the cubic diamond crystalline ordering as well as the local ordering in liquid phases are well captured by the choice of $l = 3$ and the average value of q_3 varies between 0.2 (high temperature liquid phase) and 0.75 (cubic diamond crystal phase). We note that if we use $l = 6$, the results discussed in this paper do not vary much.

C. Excess entropy

Excess entropy per atom s_E (all entropies are expressed in units of the Boltzmann constant k_B, per atom; thus, $s_E = S_E/Nk_B$ in terms of the total excess entropy S_E) is defined as $s_E = s - s_{id}$, where s is the total entropy of the system per atom and s_{id} is the entropy per atom of an ideal gas system. To compute the total entropy we perform thermodynamic integration of appropriate derivatives of the free energy. The details of the thermodynamic integration path are provided in the Appendix.

A two body approximation to the excess entropy has been calculated from the pair correlation function[39,40] and is given by

$$s_2 = -2\pi\rho \int_0^{\infty} \{g(r)\ln(g(r)) - [g(r) - 1]\} r^2 dr, \tag{10}$$

where $g(r)$ is the pair correlation function, and ρ is the number density. Previous simulation studies on model water and silica report that qualitatively the pair correlation entropy s_2 compares well with the total excess entropy s_E.[27,28,30] We present a similar comparison of the two measures of excess entropies in this work for liquid silicon.

III. RESULTS

From the previous study of the phase diagram of supercooled silicon,[13] we recognise that the state points at which we compute various quantities are in liquid and high density

supercooled liquid phase. We begin by presenting our results related to the anomalous behaviour in the dynamics of the system.

A. Anomaly in diffusion coefficient

The anomalous behaviour in diffusion is characterised by an increase in diffusivity with an increase in pressure or density. In Fig. 1 we show diffusivity as a function of density and pressure for different temperatures. The isotherms ranging between $T = 1070$ K and $T = 2517$ K show a maximum in diffusivity and the locus of maxima, in the phase diagram, will divide the regions of anomalous and normal behaviour in D. For temperatures between $T \geq 2895$ K and $T \leq 3147$ K, we have performed isothermal-isochoric MD simulations since the system is prone to cavitations in isothermal-isobaric MD simulations. For temperatures beyond 3147 K, approaching the liquid spinodal, we do not find maximum in D before the system cavitates. The locus of diffusivity minima marks the lower bound of anomalous region and is expected to be found at low temperatures close to the spinodal, where system's dynamics is slow and crystallisation rates are high and we have not attempted to find this locus in our study.

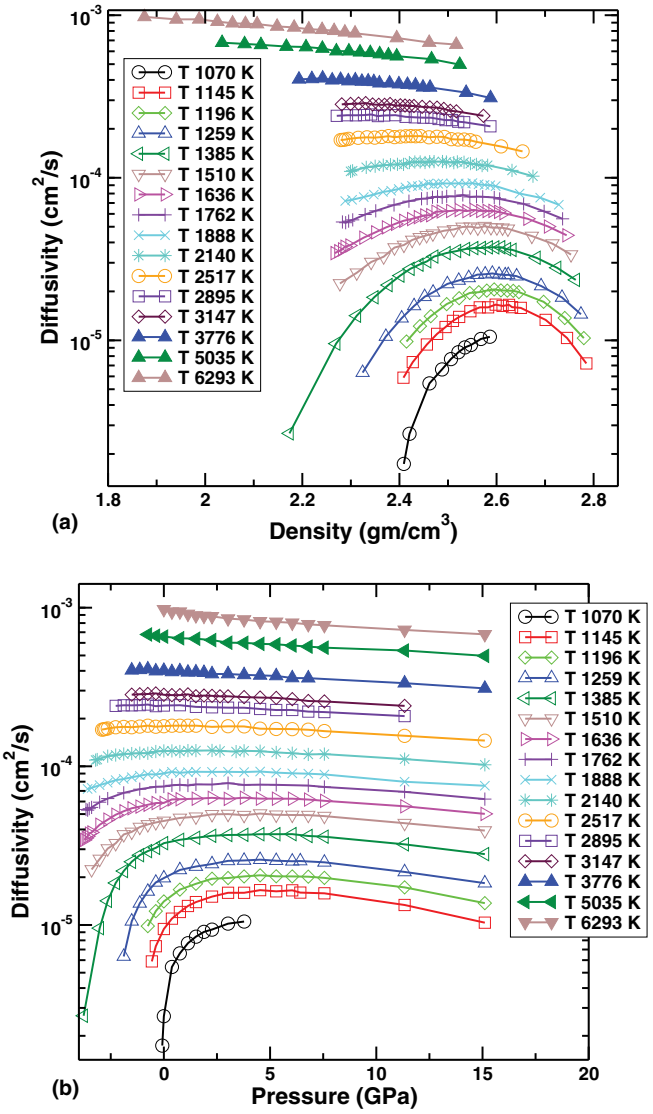

FIG. 1. Diffusivity as a function of (a) density and (b) pressure for different temperatures obtained from MD simulations of Stillinger-Weber silicon. The maximum in diffusivity demarcates the regions of normal and anomalous behaviour in phase diagram.

B. Behaviour of structural order parameters

Here we present our results related to the change in structural order parameters in the liquid and supercooled liquid phases, with a focus on the anomalies in structural change. In Fig. 2(a) we show the distribution of the tetrahedrality order parameter q_{tetra} obtained from equilibrium NPT MD runs along the $P = 0$ GPa isobar for temperatures varying from high T liquid phase to supercooled high density liquid (HDL) phase to low density liquid (LDL) phase (at $T = 1057$ K). As observed in previous work on water[9] and silica,[10] the q_{tetra} distribution shows a weak bimodal behaviour in the high temperature phase (indicative of transient tetrahedral and non-tetrahedral local structures). With a decrease in temperature, approaching the liquid-liquid transition (at $T = 1060$ K for $P = 0$ GPa), the major peak of the distribution move towards the value 1. In the HDL phase at $T = 1070$ K we find a broad q_{tetra} distribution and in the LDL phase at $T = 1057$ K, since the majority of the atoms are locally four coordinated we find a unimodal distribution. In Fig. 2(b) we show q_{tetra} distribution along the $T = 1196$ K isotherm for pressures varying between 19.1 GPa and -1.51 GPa (approaching the Widom line or locus of compressibility maxima). Similar to the trend along the $P = 0$ GPa isobar we find a bimodal distribution at high pressures, which weakens with a decrease in pressure. At pressure $= -1.51$ GPa, even though the liquid is in the low-density phase, we find the presence of a small percentage of 5-coordinated particles (contributing to a weak bimodal distribution). Simulation work on water has shown that the mobility of water molecules has been facilitated by the defect particles[11] and it would be interesting to do similar analysis in silicon.

In Figs. 3(a) and 3(b) we show the distribution of local orientational order q_3 along $P = 0$ GPa isobar and $T = 1196$ K isotherm. In contrast to the q_{tetra} distribution, we find that the q_3 distribution shows a clear bimodal distribution at all temperatures and pressures. The local orientational order q_3, by definition, considers all the nearest neighbours instead of first four nearest neighbours, and seems to capture the changes in local environment better than the tetrahedrality order parameter.

In Fig. 4 we show the average q_{tetra} as a function of density and pressure for different temperatures. In the range of temperatures varying between $T = 1070$ K and $T = 3147$ K, we find that q_{tetra} decreases with the increase in density (or pressure) which is termed anomalous since normally one expects the structural order to increase with the compression. We do not find a maximum in q_{tetra} in the range of state points we have analysed (which would have bound the region of structural anomaly according to the definition of Errington and Debenedetti[9]). At high temperatures ($T > 3776$ K), we find normal behaviour in q_{tetra} where the order parame-

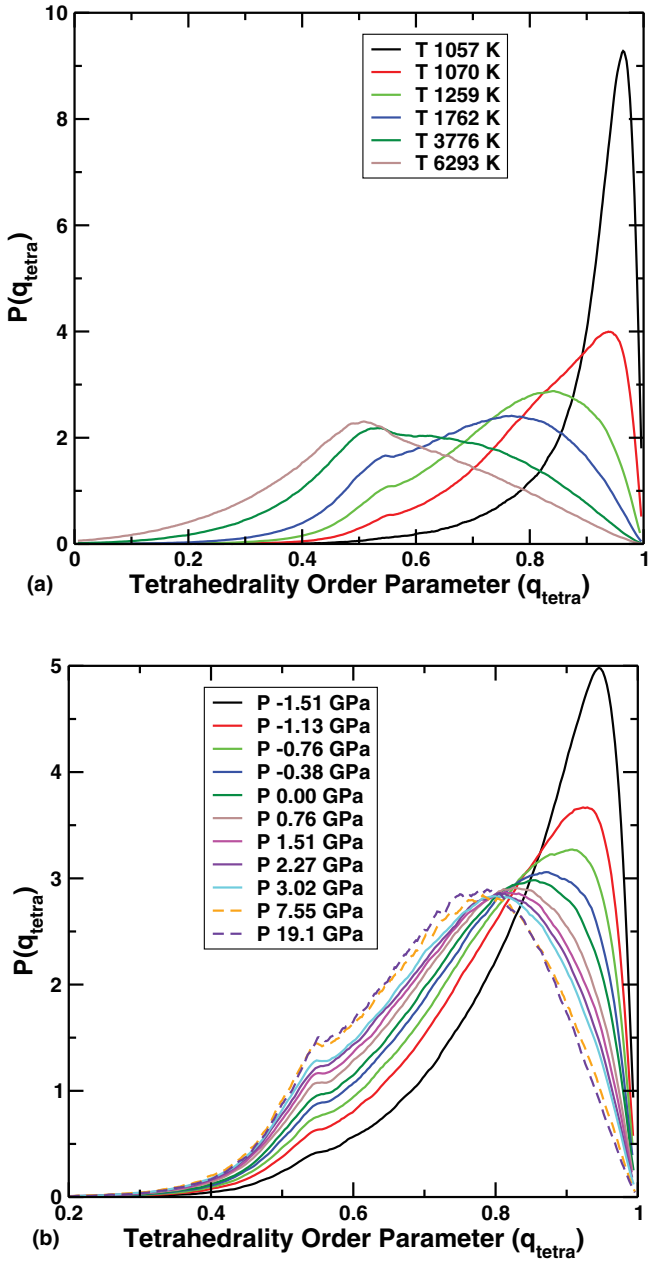

FIG. 2. Distribution of tetrahedrality order (q_{tetra}) obtained from MD simulations of Stillinger-Weber silicon along (a) $P = 0$ GPa isobar for the high T liquid, high density (HDL), and low density supercooled liquid phases. The high T liquid and HDL phases show bimodal distributions, whereas the LDL phase shows unimodal distribution peaked near 1. (b) $T = 1196$ K isotherm for varying pressures. Bimodal distribution at high pressures weakens with a decrease in pressure.

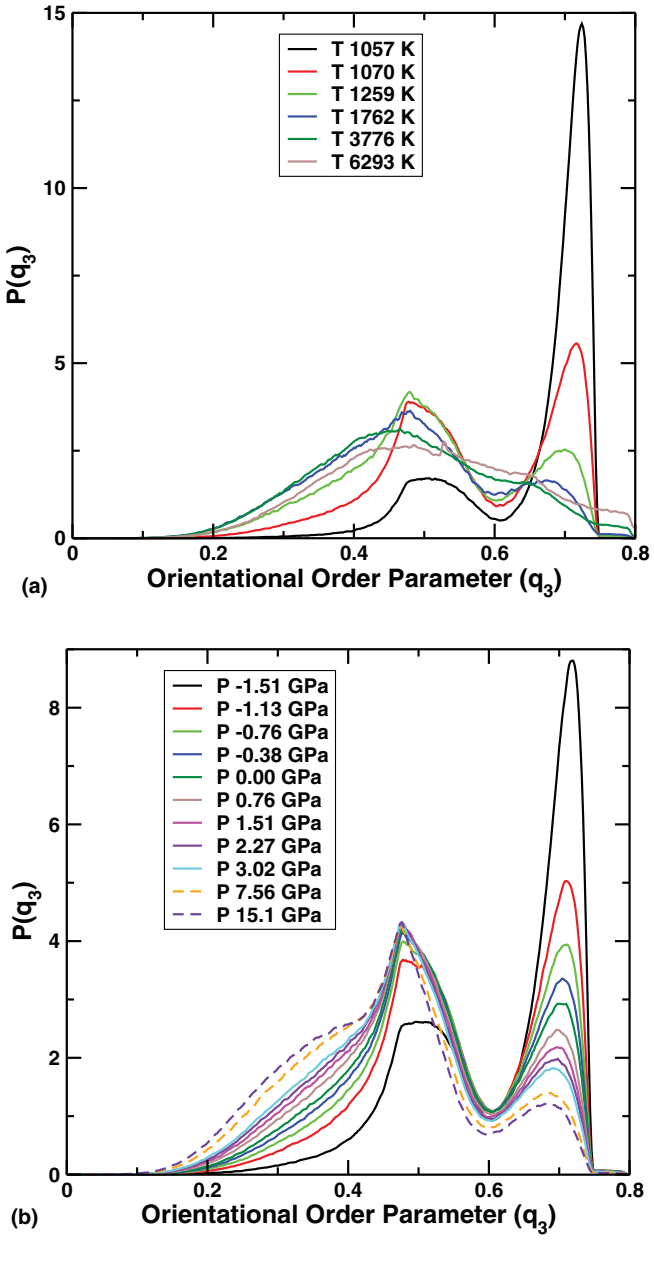

FIG. 3. Distribution of local orientational order parameter (q_3) obtained from MD simulations of Stillinger-Weber silicon along (a) $P = 0$ GPa isobar for high T liquid, high density (HDL), and low density (LDL) supercooled liquid phases. (b) Along $T = 1196$ K isotherm. Bimodal distribution is found at all the temperatures and pressures, but is smeared out at high temperatures and pressures.

ter increases with density (or pressure). At high densities ($\rho > 2.6$ gm/cm^3), in the range of temperature varying between $T = 1070$ K and $T = 2140$ K we find that the q_{tetra} goes through a minimum. At these state points, since the coordination number is around 6, an increase in tetrahedral order is unexpected. Since the computation of q_{tetra} considers the first four nearest neighbours, it can be ambiguous if the first coordination shell has more than 4 atoms at equal distances from a reference atom. Hence an increase in tetrahedral ordering at these state points can be an artefact of the definition of tetrahedrality order parameter. Unlike q_{tetra}, the orientational order parameter q_3 considers all the neighbouring atoms. In Fig. 5 we show the average q_3 as a function of density and pressure for different temperatures. We find that in the whole range of state points we have analysed, average q_3 shows an anomalous behaviour wherein the orientational order increases with the decrease in density (or pressure) including at high densities.

In Fig. 6 we show the average translational order parameter t_{trans} as a function of density and pressure. For all temperatures less than $T = 2517$ K, we find that with the lowering of density (or pressure) the translational order decreases and goes through a minimum. Errington and Debenedetti,[9] in their work, suggest that a minimum in the translational order

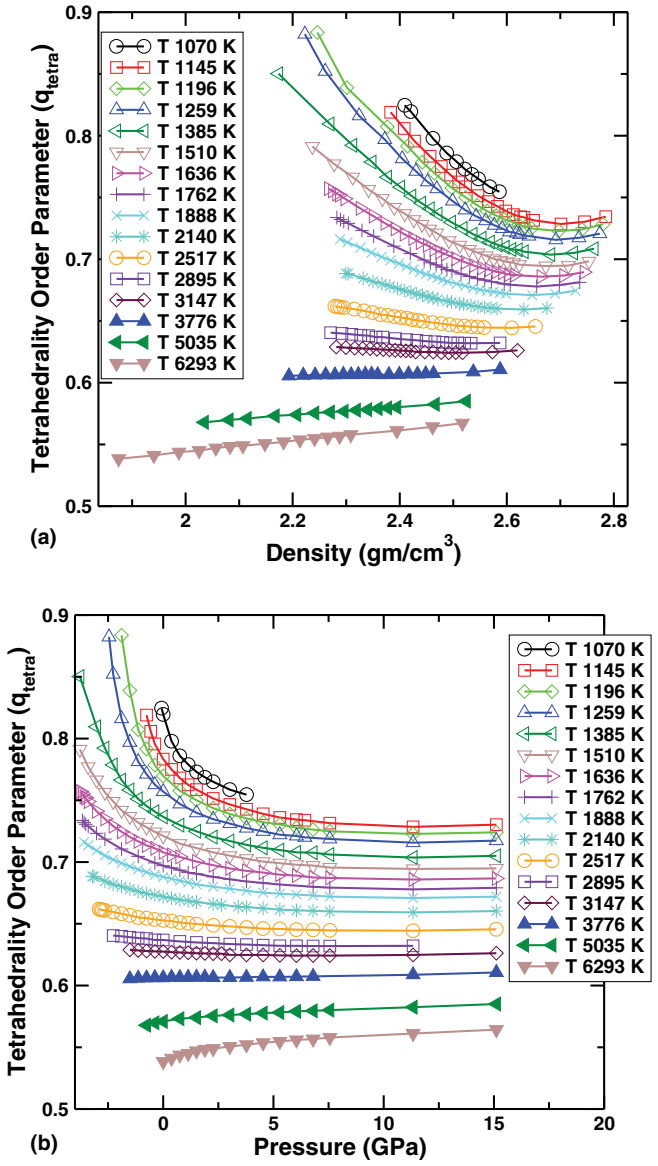

FIG. 4. The average tetrahedrality order q_{tetra} as a function of (a) density and (b) pressure for different temperatures obtained from MD simulations of Stillinger-Weber silicon. The tetrahedrality order increases with decrease in density and pressure for temperatures varying between $T = 1070$ K and $T = 3147$ K and at high temperatures ($T > 3776$ K), a normal behaviour in q_{tetra} is found where the order parameter increases with density and pressure. At high densities ($\rho > 2.6$ gm/cm^3), in the range of temperature varying between $T = 1070$ K and $T = 2140$ K the q_{tetra} goes through a minimum.

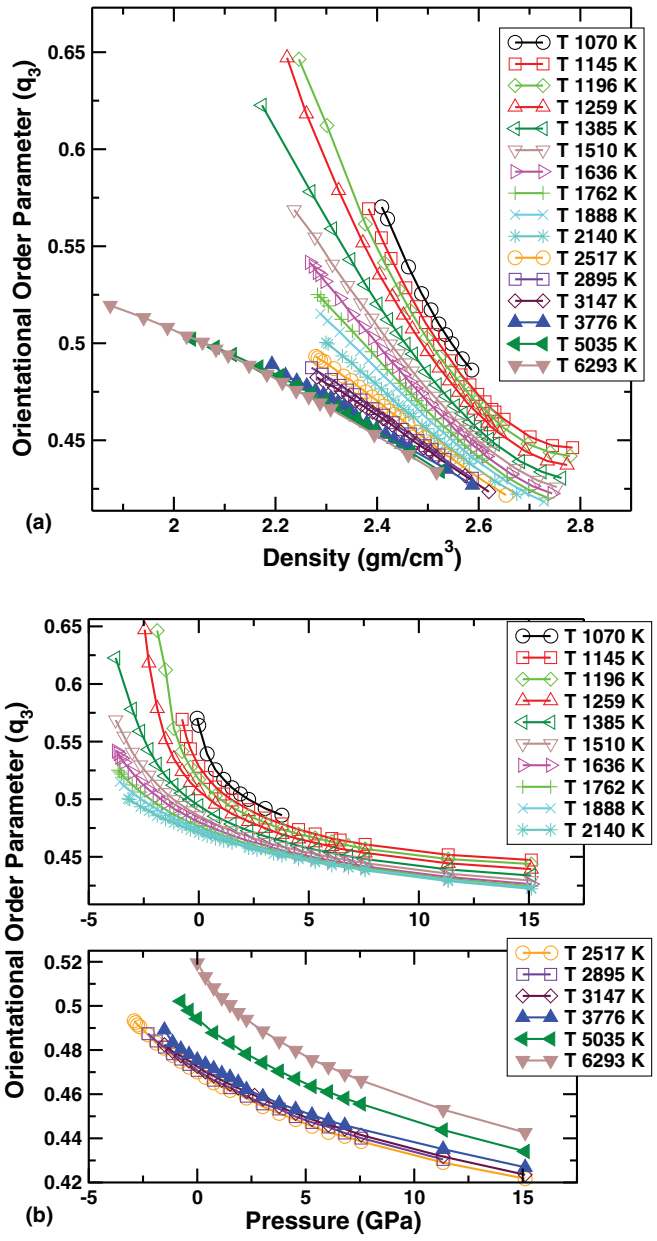

FIG. 5. The average local orientational order q_3 as a function of (a) density and (b) pressure for different temperatures obtained from MD simulations of Stillinger-Weber silicon. In the whole range of state points, the local orientational shows an anomalous behaviour in which order increases with decrease in density.

defines the onset of anomalous behaviour in structural order. For temperatures greater than $T = 2517$ K we encounter the liquid spinodal and hence the system cavitates in the NPT MD runs before t_{trans} goes through a minimum. Curiously at very high temperatures ($T > 5000$ K, beyond the liquid gas critical point) we once again find that the t_{trans} goes through a minimum.

Next we analyse the correlation between translational order parameter and orientational order parameters. In Fig. 7 we show the parametric plot of t_{trans} against q_{tetra}. We find that in the structurally anomalous region there is tight correlation between the two order parameters and also there are no state points which lie below region of tight correlation, both features similar to water.[9] In Fig. 8(a) we show the parametric plot of t_{trans} against q_3 where we find that the tight correlation between the two order parameters is absent. We note that in silica, Shell *et al.*[10] do report a similar result and in their work they use the tetrahedrality order parameter considering six nearest neighbours. To obtain a better understanding of this feature, we calculate the q_3 order parameter by considering only the first four nearest neighbours (see Fig. 8(b)) and we indeed get back the feature of correlation between the two structural orders.

From these analyses pertaining to the structural order parameters we wish to highlight that (a) at intermediate temperatures and densities, the features of the structural order

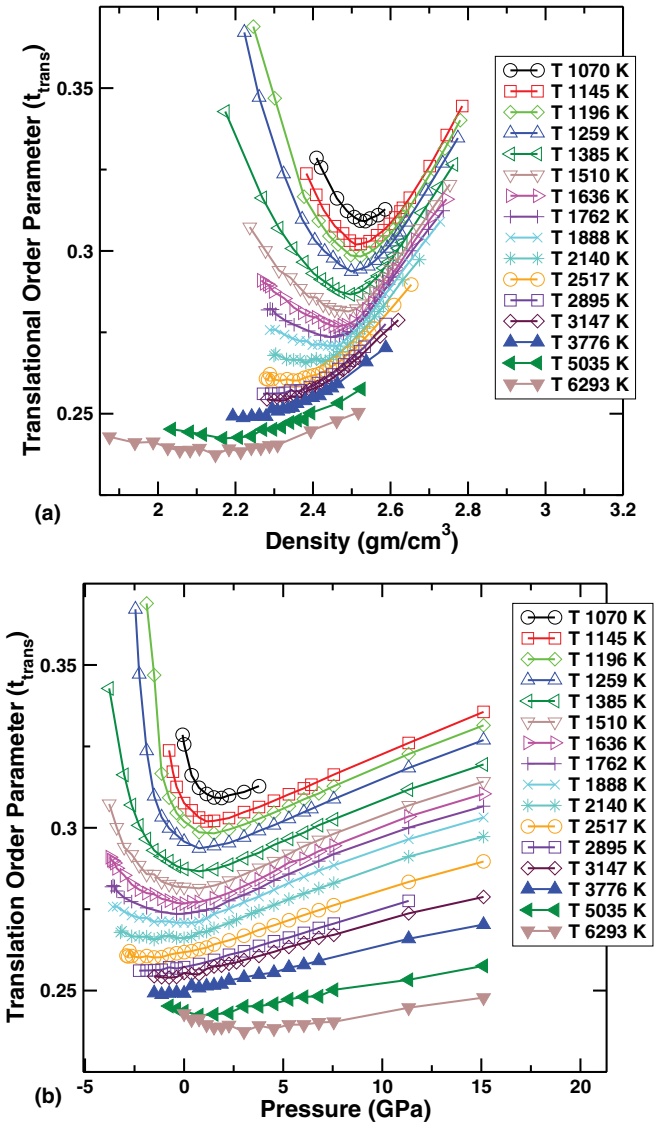

FIG. 6. The average translational order t_{trans} as a function of (a) density and (b) pressure for different temperatures obtained from MD simulations of Stillinger-Weber silicon. At low pressures and densities, the translational order goes through a minimum indicating at an onset of structural anomaly. Curiously at very high temperatures ($T > 5000$ K, beyond the liquid gas critical point) the translation order again goes through a minimum.

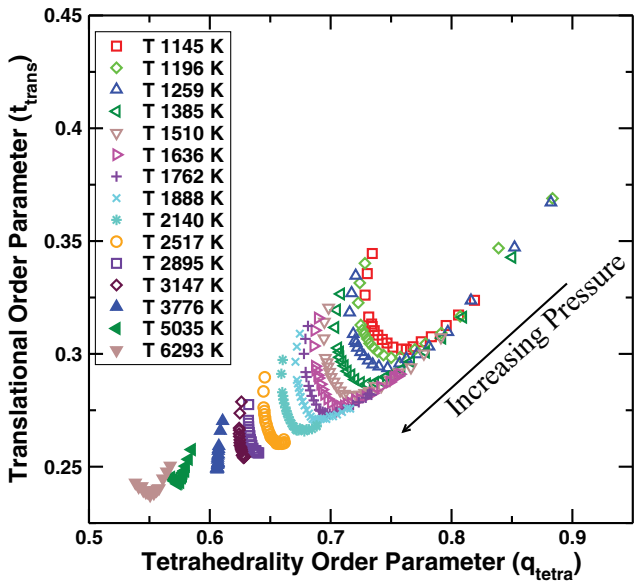

FIG. 7. Parametric plot of translational order t_{trans} against the tetrahedrality order t_{tetra} for different temperatures obtained from MD simulations of Stillinger-Weber silicon. The arrow represents the direction of increase in pressure for each temperature. A tight correlation between the two order parameter is seen in the region of structural anomaly.

parameters are similar to that of water and silica, (b) the translational order parameter, using which onset of structural anomaly is defined, goes through a minimum beyond the liquid-gas critical point, (c) the tetrahedrality order parameter fails to capture the precise local tetrahedral order if the first coordination shell has more than 4 atoms at equal distances from a reference atom, and (d) the feature of structural order parameters being related to each other in the structurally anomalous region depends on the method of computation of orientational order parameter.

C. Nesting of anomalies

Having computed the loci of diffusivity maxima and translational order minima we have located the onset of dynamical and structural anomalies in the phase diagram of liquid silicon. We note that the locus of density maxima, which represents the onset of thermodynamic anomaly was reported in the work of Vasisht *et al.*[13] In Fig. 9 we show these loci, which constitute the *nesting* of different anomalous regions, in (T, ρ) and (P, T) planes. The cascading of different regions of anomaly is similar to that of silica—region of diffusivity anomaly encloses the region of structural anomaly which in turn encloses the region of thermodynamic anomaly. At low temperatures and high pressures, the regions of structural anomaly and thermodynamic anomaly reverse in order.

We next present our results related to excess entropy and its relation with the above discussed anomalies.

D. Excess entropy

The excess entropy by definition ($S_E = S - S_{id}$) characterises the reduction in the accessible states relative to an ideal gas, due to inter-particle correlations. The contribution of inter-particle correlations can be broken up into two-body term, three-body term, etc., and the translational order is a measure of the two-body correlations. Errington and coworkers[28] argue that the region in the phase diagram where the excess entropy anomalously increases with decrease in density is also the region where translational order anomaly is observed. Hence the criterion to observe structural anomalies can be written in terms of $\ln(\rho)$ as $(\partial s_E/\partial \ln(\rho))_T > 0$.

The excess entropy is associated with the density following the thermodynamic relation[41]

$$\left(\frac{\partial \rho}{\partial T}\right)_P = \rho^2 \left(\frac{\partial \rho}{\partial P}\right)_T \left(\frac{\partial s}{\partial \rho}\right)_T, \tag{11}$$

where s is the total entropy of the system. The condition for anomalous density is that $\partial\rho/\partial T|_P$ should be greater than zero. Since the compressibility is a positive definite quantity for

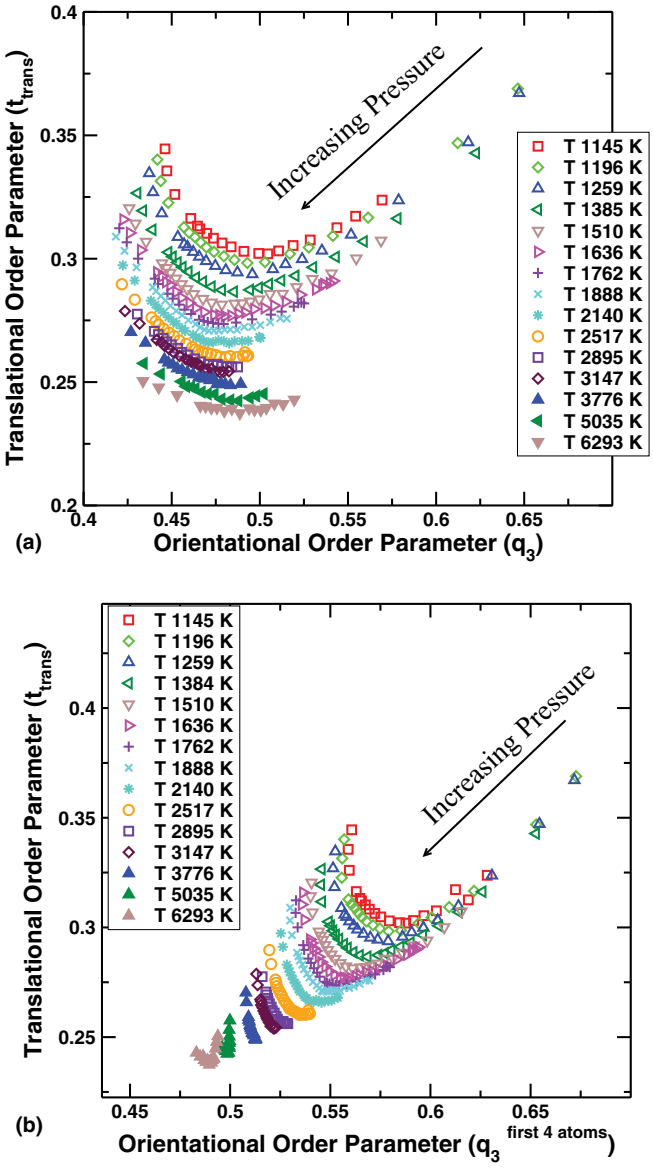

FIG. 8. Parametric plot of translational order t_{trans} against (a) the local orientational order parameter q_3 and (b) the local orientational order calculated using the first four nearest neighbours for different temperatures obtained from MD simulations of Stillinger-Weber silicon. In the region of structural anomaly, a tight correlation between t_{trans} and q_3 is not observed. But when q_3 computed using first four nearest neighbours is used, the correlation is evident. The arrow represents the direction of increase in pressure for each temperature.

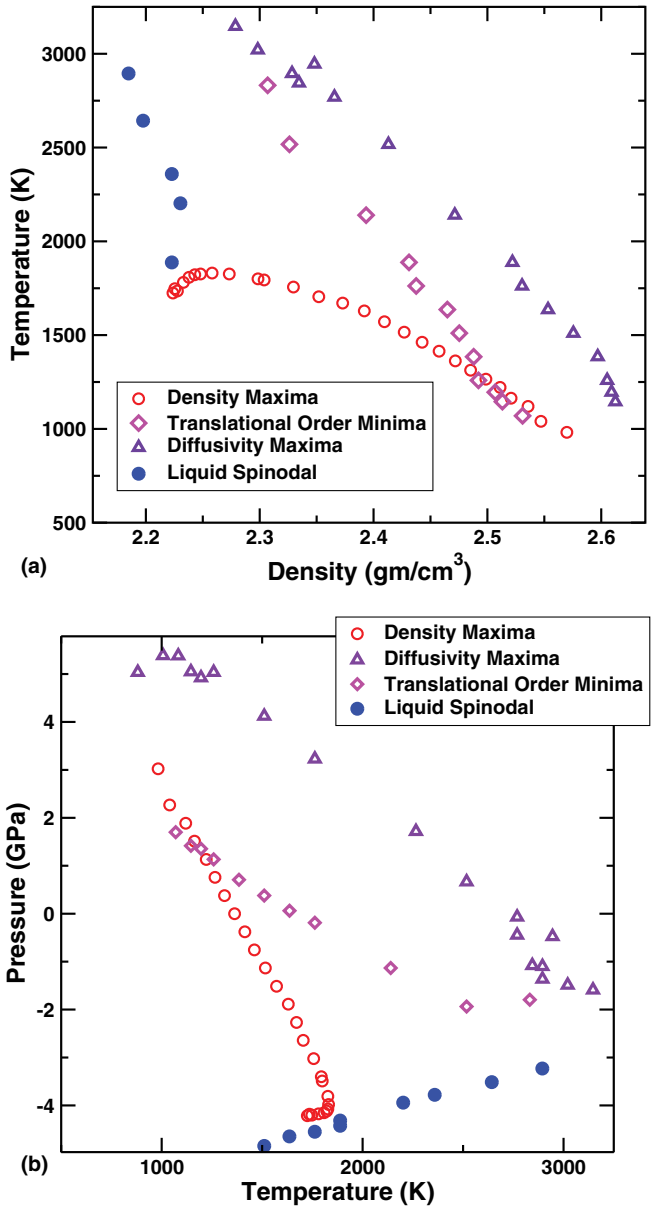

FIG. 9. (a) Phase diagram of Stillinger-Weber silicon in (T, ρ) plane showing the loci of density maxima, translational order minima and diffusivity maxima along with the liquid spinodal. (b) Phase diagram of liquid silicon in (P, T) plane showing the loci of density maxima, translational order minima and diffusivity maxima along other features of the phase diagram.

an equilibrium system, one can deduce from the above equation that for system showing density anomaly should satisfy the condition $(\partial s/\partial \rho)_T > 0$. Since $s_E = s - s_{id}$, where $s_{id} = -\ln(\rho) + C(T)$ with $C(T)$ being purely temperature dependent, by taking a partial derivative with respect to $\ln(\rho)$ of s_E at a constant temperature we get

$$\left(\frac{\partial s_E}{\partial \ln(\rho)}\right)_T = \left(\frac{\partial s}{\partial \ln(\rho)}\right)_T + 1. \quad (12)$$

The above equation shows that to observe anomalous density variation with temperature, $(\partial s_E/\partial \ln(\rho))_T$ should be greater than 1.

Even though there are no rigorous thermodynamic relations which associate the diffusivity with the excess entropy, the empirical scaling relation proposed by Rosenfeld[42] expresses the diffusion coefficient as a function of the excess entropy, as

$$D^* = a_D \exp(b_D s_E), \quad (13)$$

where the reduced diffusion coefficient is $D^* = D\rho^{1/3}/(k_B T/m)^{1/2}$, D is the diffusion constant, m is the mass of the particle, and ρ is the number density.

Dzugutov[43] has proposed another scaling relation connecting the reduced diffusion coefficient, defined using the collision frequency, $D_z^* = D\Gamma^{-1}\sigma^{-2}$ with the excess entropy

TABLE I. The table summarising the criteria for observing the onset of density, structural, and diffusivity anomalies. The constant C is obtained from the scaling relation which relates the diffusion coefficient with the excess entropy.

Structural	$(\frac{\partial s_E}{\partial ln(\rho)})_T > 0$
Density	$(\frac{\partial s_E}{\partial ln(\rho)})_T > 1$
Diffusivity	$(\frac{\partial s_E}{\partial ln(\rho)})_T > C$

s_E as

$$D_z^* = a_0 \exp(s_E), \tag{14}$$

where the collision frequency $\Gamma = 4\sigma^2 g(\sigma)\rho\sqrt{\pi k_B T/m}$, σ is the hard-sphere diameter, $g(\sigma)$ is the value of radial distribution function at the contact distance. In the original paper of Dzugutov[43] the above relation was tested using the two-body excess entropy S_2. In simulations of soft spheres, σ was interpreted as the position of first peak of radial distribution function.

Taking the partial derivative of the scaling relation, Eq. (13), with respect to $\ln(\rho)$ and rearranging the terms, we get

$$\left(\frac{\partial s_E}{\partial \ln(\rho)}\right)_T = \frac{C}{3b_D}, \tag{15}$$

where $C = 1 + 3(\frac{\partial \ln(D)}{\partial \ln(\rho)})_T$.

At the diffusivity maxima the derivative $(\frac{\partial \ln(D)}{\partial \ln(\rho)})_T = 0$. Hence the criterion to observe anomalous diffusivity would be $(\partial s_E/\partial \ln(\rho))_T > 1/(3|b_D|)$. The system dependent constant b_D obtained as the exponent of Rosenfeld scaling relation varies between 0.8 and 1.7.[14,42,44,45]

If we extend the above argument to Dzugutov scaling relation, Eq. (14), we get

$$\left(\frac{\partial s_E}{\partial \ln(\rho)}\right)_T = C_z, \tag{16}$$

where $C_z = (\frac{\partial \ln(D)}{\partial \ln(\rho)})_T - 1$. Hence the diffusivity anomaly criterion should be $(\partial s_E/\partial \ln(\rho))_T > -1$. In Table I we summarise the above criteria for observing the onset of different anomalies.

To begin with we present the per particle excess entropy s_E (see Fig. 10) and the pair correlation entropy s_2 (see Fig. 11) as a function of pressure and density for different isotherms. In both the measures of excess entropy (s_E and s_2) we find an anomalous region in the phase diagram (for temperatures varying between $T = 1070$ K and 1762 K), wherein the excess entropy increases with an increase in density (or pressure) at constant temperature. The estimates of s_2 are smaller in magnitude than s_E which is expected (since we are ignoring the contribution of other correlation functions like 3-body, etc.), but the profiles as a function of density and pressure are quite similar. To know the extent of proportionality between these two measures of excess entropy, in Fig. 12(a), we show s_2 against s_E and the ratio s_2/s_E as a function of pressure in the inset of Fig. 12(a). We also show in Figs. 12(b) and 12(c), this ratio as a function of temperature for different isobars as well as isochores. From these plots we infer broadly that with the increase in temperature the proportionality between the two measures of excess entropy increases, but the ratio s_2/s_E increases with increasing density for $T < 3000$ K whereas at higher temperatures the ratio increases with decreasing density. This is expected since in the low temperature/high density, high temperature/low density regions (as is clear at least using q_{tetra}), we find a reduction in orientational order, and hence expect a reduction of its contribution to excess entropy and domination of two-body correlation contribution. In fact a recent work of Singh and coworkers[38] reports explicit computation of the three-body contribution to excess entropy Stillinger-Weber liquids (at $\lambda = 16$ and $\lambda = 23.15$). They find that for $\lambda = 23.15$, at low temperatures the magnitude of three-body excess entropy is higher than that of two-body and at temperature above the melting point, the two-body excess entropy has a bigger magnitude

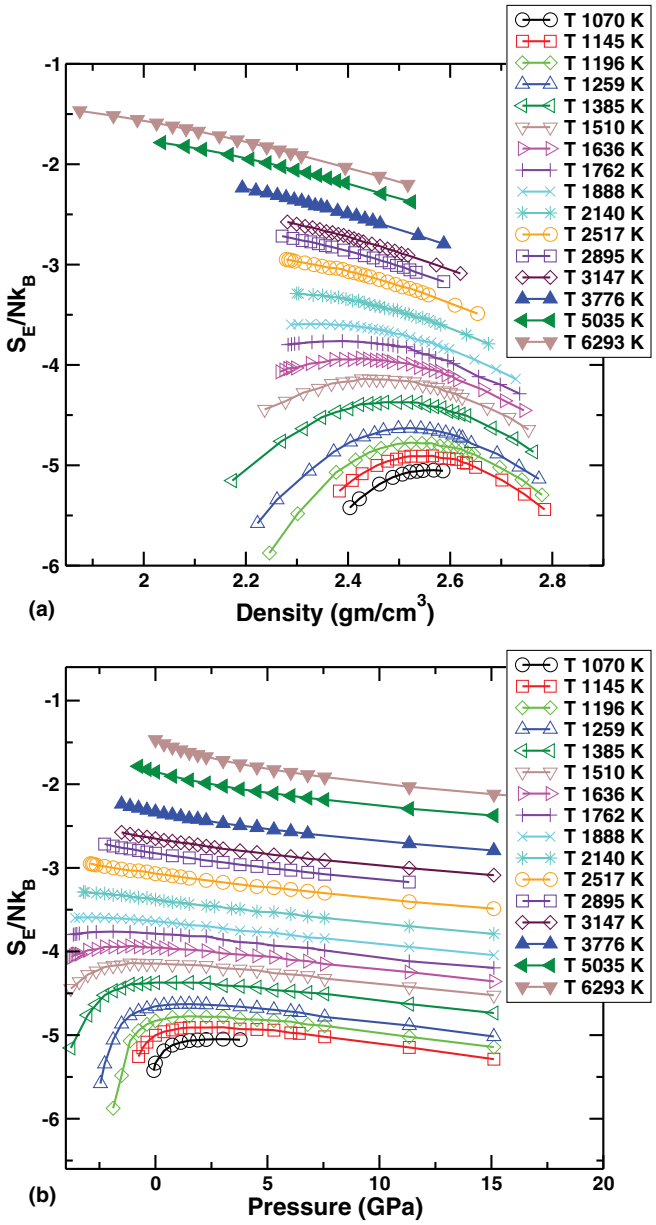

FIG. 10. Total excess entropy s_E of Stillinger-Weber silicon as a function of (a) density and (b) pressure for different temperatures obtained from thermodynamic integration. Excess entropy shows an anomalous behaviour wherein it increases with an increase in density, for temperature ranging between $T = 1070$ K and 1762 K, before going through a maximum.

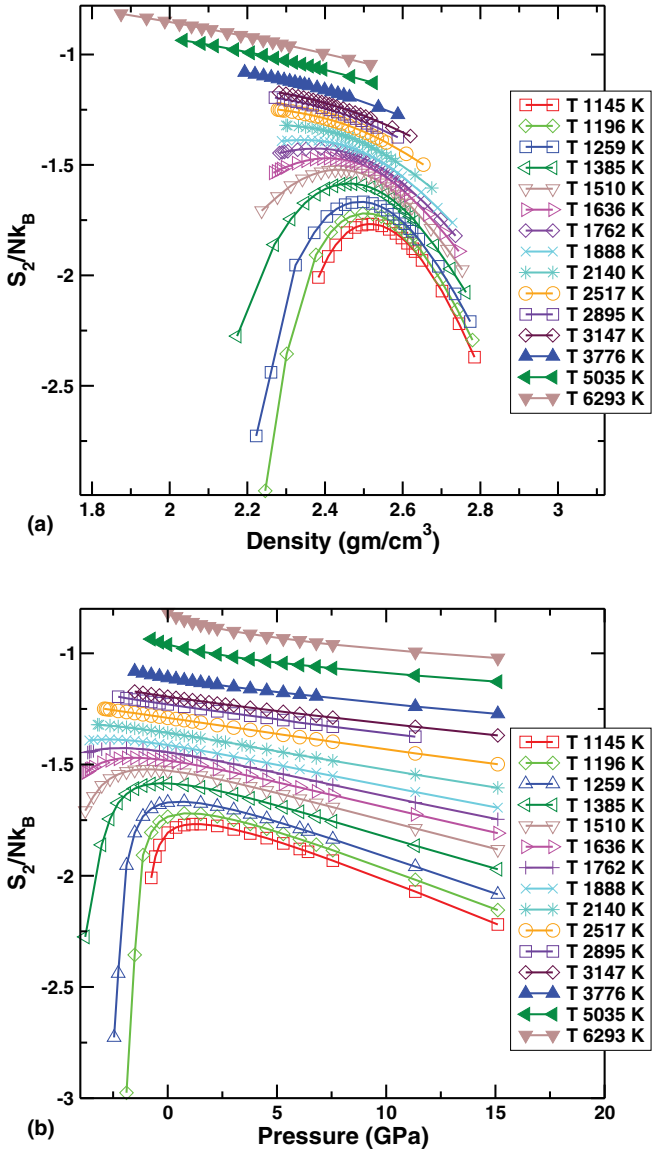

FIG. 11. Pair correlation entropy s_E of Stillinger-Weber silicon as function of (a) density and (b) pressure for different temperatures obtained from radial distribution function. Similar to the total excess entropy, the pair correlation entropy anomalous behaviour for temperature ranging between $T = 1070$ K and 1762 K, before going through a maximum.

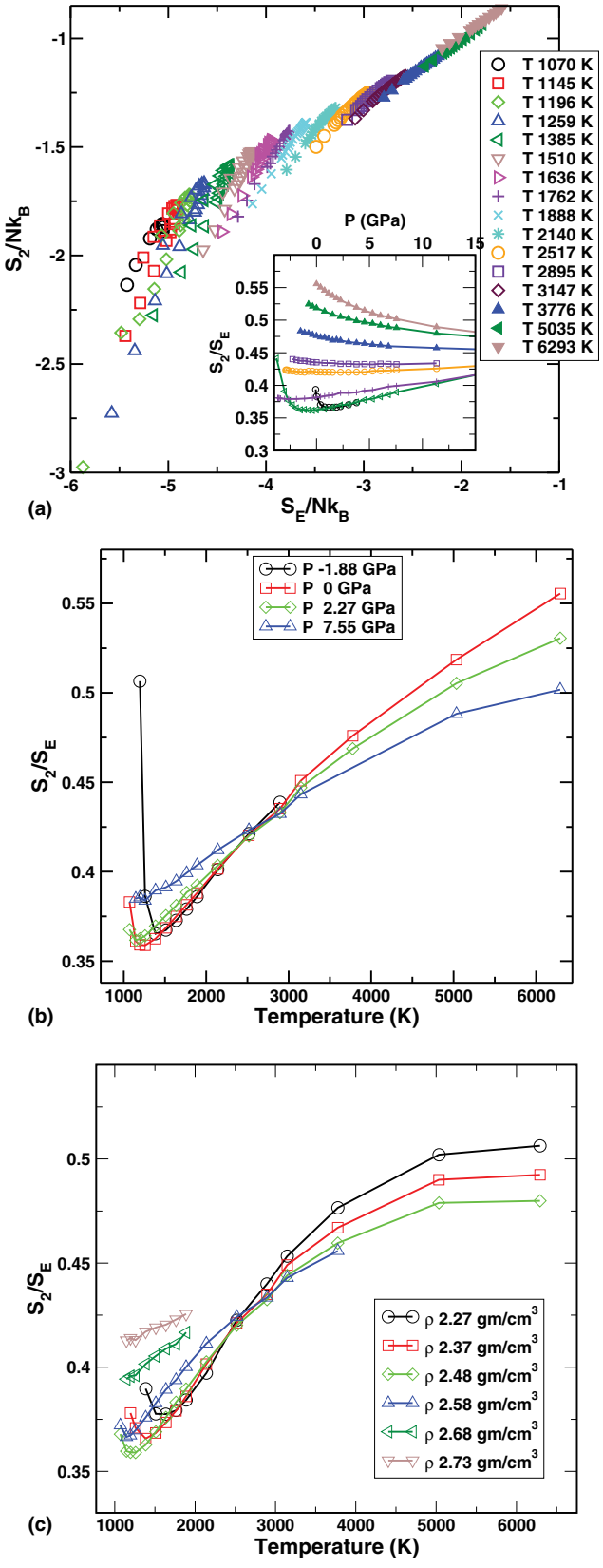

FIG. 12. (a) Pair correlation entropy against the total excess entropy for different isotherms. (Inset) The ratio of the two measures of entropy as a function of pressure for different isobars. (b) The ratio of the two measures of entropy as a function of temperature for different isobars and (c) different isochores. At low temperatures/high densities and high temperatures/low densities, the proportionality between the two measures of excess entropy is considerably better than at low temperatures/low densities and high temperatures/high densities, respectively.

than the three-body. At temperatures below 1385 K for low pressure values ($P < 1$ GPa), we find that the ratio of s_2 to s_E increases, which is an interesting observation which needs to be investigated further.

Focusing back on the relation between excess entropy and anomalies, we first present the results related to excess entropy, structural anomaly, and thermodynamic anomaly. The criterion to observe structural anomaly in the phase diagram is $\partial s_E/\partial \ln(\rho)|_T > 0$ and hence the onset temperature and density for structural anomaly (corresponding to minimum in translational order) corresponds to $\partial s_E/\partial \ln(\rho)|_T = 0$ (maximum in excess entropy).[16,28] Similarly the temperature and density associated with density maxima corresponds to $\partial s_E/\partial \ln(\rho)|_T = 1$.[28] In Fig. 13 we show the partial derivative of excess entropy as a function of density for different isotherms. The isotherms which intersect the horizontal lines satisfy the

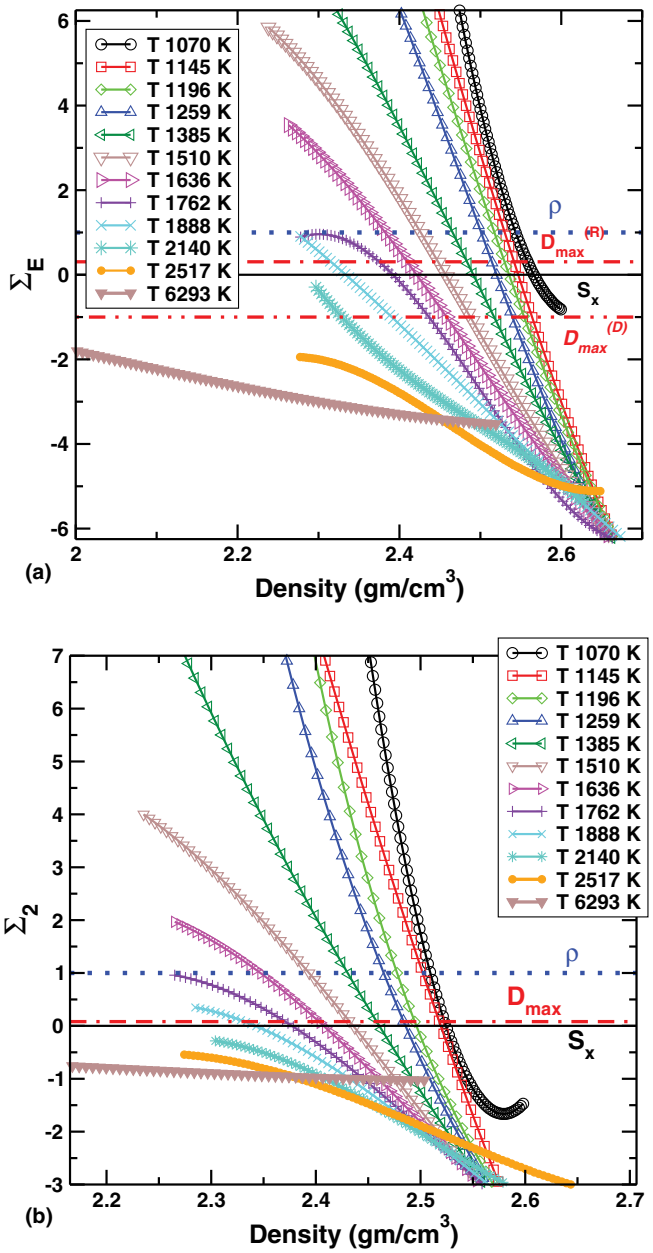

FIG. 13. (a) Partial derivative of the total excess entropy with respect to the logarithm of density $\Sigma_E = \partial s_E/\partial \ln(\rho)|_T$ as a function density for a set of isotherms. The horizontal lines correspond to excess entropy based criterion to locate the onset of different anomalies. The solid black line (S_x) corresponds to $\Sigma_E = 0$, the double dashed-dotted red line ($D^{(R)}_{max}$ from Rosenfeld scaling) corresponds to $\Sigma_E = 0.1587$, the dashed-double dotted red line ($D^{(D)}_{max}$ from Dzugutov scaling) corresponds to $\Sigma_E = -1$, and the dotted blue line (ρ) corresponds to $\Sigma_E = 1.0$. (b) Partial derivative of the pair correlation entropy with respect to the logarithm of density Σ_2 as a function of density for a set of isotherms. In this plot solid black line (S_x) corresponds to $\Sigma_2 = 0$, the double dashed-dotted red line (D_{max}) corresponds to $\Sigma_2 = 0.0827$, and the dotted blue line (ρ) corresponds to $\Sigma_2 = 1.0$.

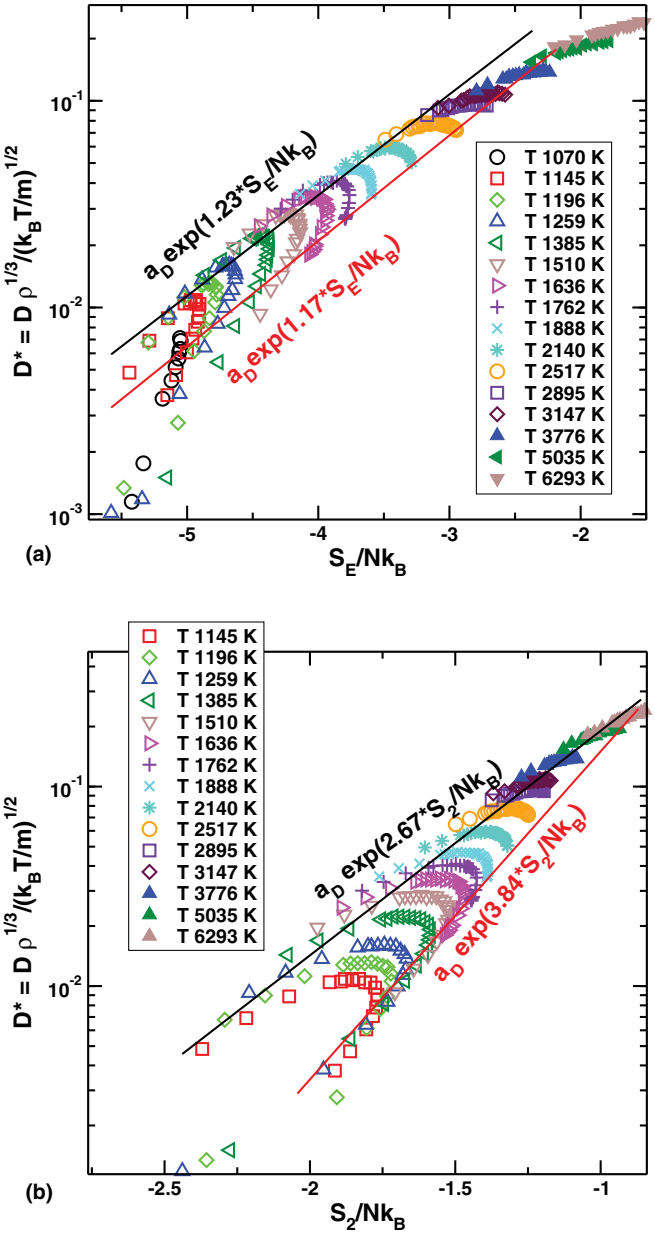

FIG. 14. Rosenfeld scaling: The reduced diffusion coefficient against the two measures of excess entropy for different isotherms. In both measures of entropy, two branches in scaling are observed, one corresponding to normal behaviour and another to anomalous behaviour, which suggests a non-trivial scaling relation between the dynamics and excess entropy.

criterion discussed above, using which we extract the temperature and density (and pressure from the equation of state) corresponding to onset of structural anomaly and density maxima.

To understand the relation between excess entropy and diffusivity anomaly, first we study the scaling relations which relate the transport properties with the excess entropy. The scaling relations are defined so as to remove the contributions arising due to the change in temperature and density changes and hence expected to obtain a set of data which collapse on to a master curve. In Figs. 14–16, we show the reduced diffusion coefficient D* (as defined by Rosenfeld[42]) as a function of two measures of excess entropy for different isotherms, isochores, and isobars, respectively, and similar set of plots using the reduced diffusion coefficient D^*_Z (as defined by Dzugutov[43]) in Figs. 17–19. Along different isotherms we find that the reduced diffusion coefficients (D* and D^*_Z) against the pair correlation entropy s_2 (Figs. 14(b) and 17(b)) clearly show two separate branches in scaling, which suggests a non-trivial scaling relation between the dynamics and excess entropy. It can also be a consequence of the fact that along an isotherm,

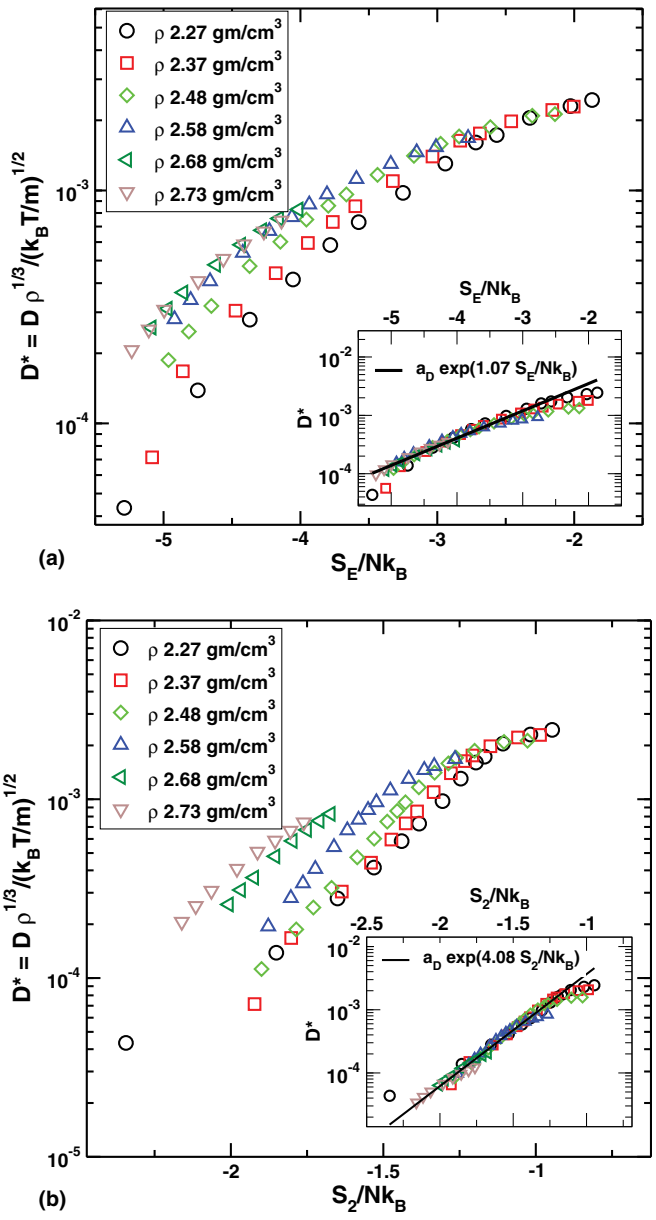

FIG. 15. Rosenfeld scaling: The reduced diffusion coefficient against the excess entropy for different isochores. All the isochores have similar fit coefficients. (Inset) The isochores collapse when the diffusivity is shifted by a constant term (by hand) and fit to a single function with an exponent of 1.07 (using S_E) and 4.08 (using S_2).

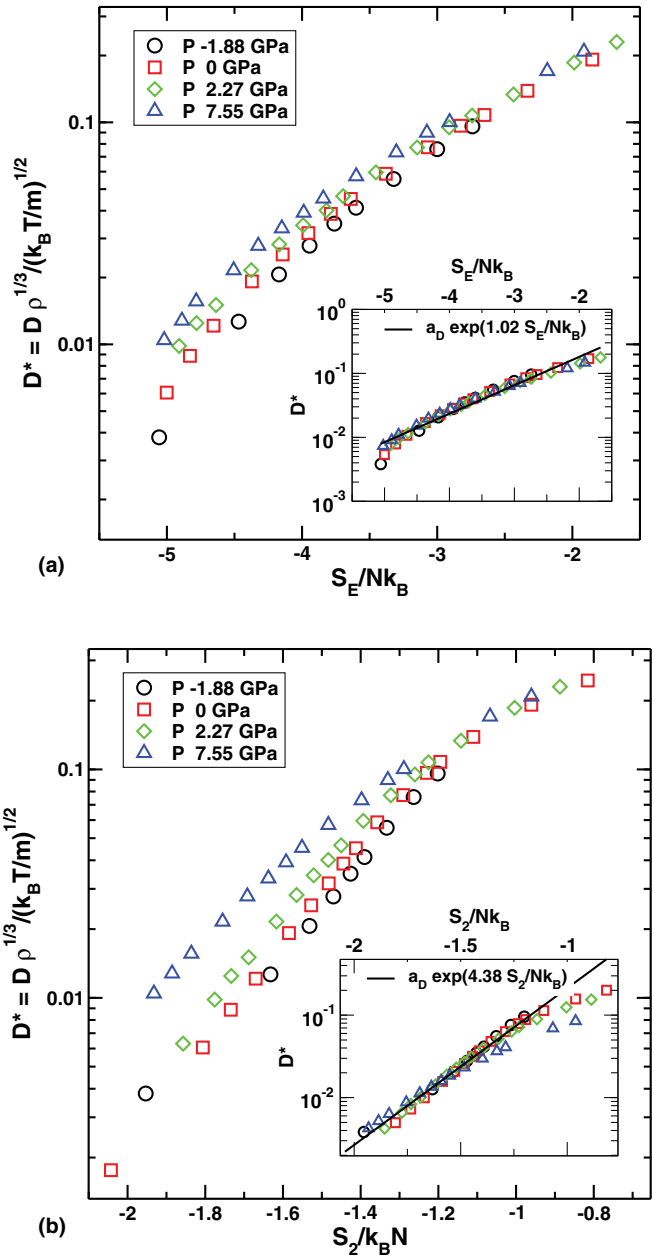

FIG. 16. Rosenfeld scaling: The reduced diffusion coefficient against the excess entropy for different isobars. All the isobars have similar coefficient b_D. (Inset) The isobars collapse when the diffusivity is shifted by a constant term (by hand) fit to a single function with a coefficient of 1.02 (using S_E) and 4.38 (using S_2).

the onset density of dynamical anomaly (maximum in D *vs.* ρ or P) differs from the onset of excess entropy anomaly (maximum in s_2 *vs.* ρ or P). A similar feature is also observed when we use total excess entropy s_E instead of pair correlation entropy s_2 (Figs. 14(a) and 17(a)). Many of the previous studies have looked at the scaling relations along isochores instead of isotherms.[16,20,23,45] In Figs. 15 and 18 we show the reduced diffusion coefficient against excess entropy along isochores. Similar to isotherms we do not find a collapsed data set, but we find that all the isochores have similar exponents (which we show in the inset of Figs. 15 and 18, where we have collapsed the isochores by shifting the diffusion coefficient by hand). We have also analysed the scaling along different isobars and find that exponents obtained from the fits are similar to that of isochores. From the tabulated exponents in Table II we find that using S_E, the exponent varies between 1.02 and 1.37 and using S_2 as a measure of excess entropy the exponent varies between 2.67 and 4.86. Previous studies, using the pair correlation entropy, show the Rosenfeld scaling exponent varies around 0.8 for hard spheres, Lennard-Jones system, water models,[42,45] between 1.3 and 1.7 for ionic melts.[23,45] For liquid metals, modeled by embedded atom models, using S_2 both Rosenfeld (with exponent 0.8) and Dzugutov scalings have been verified.[14,44] From Table II we note that (i) the exponents depend on the measure of excess entropy and (ii) the exponents obtained from isochores and isobars are similar to each other and similar to the exponents obtained from the

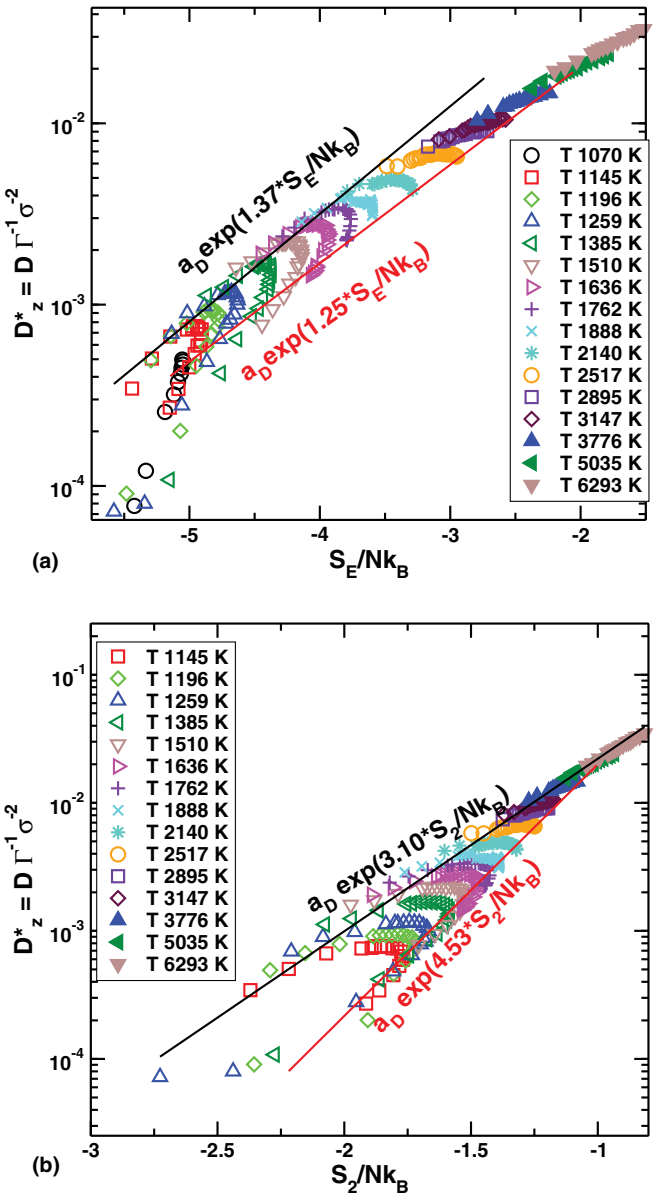

FIG. 17. Dzugutov scaling: The reduced diffusion coefficient against the excess entropy for different isotherms. The collision frequency Γ is computed using the amplitude and position of first peak of radial distribution function. The Dzugutov scaling relation ($D^*_z = a_0 \exp(s_E)$) works reasonably well using S_E.

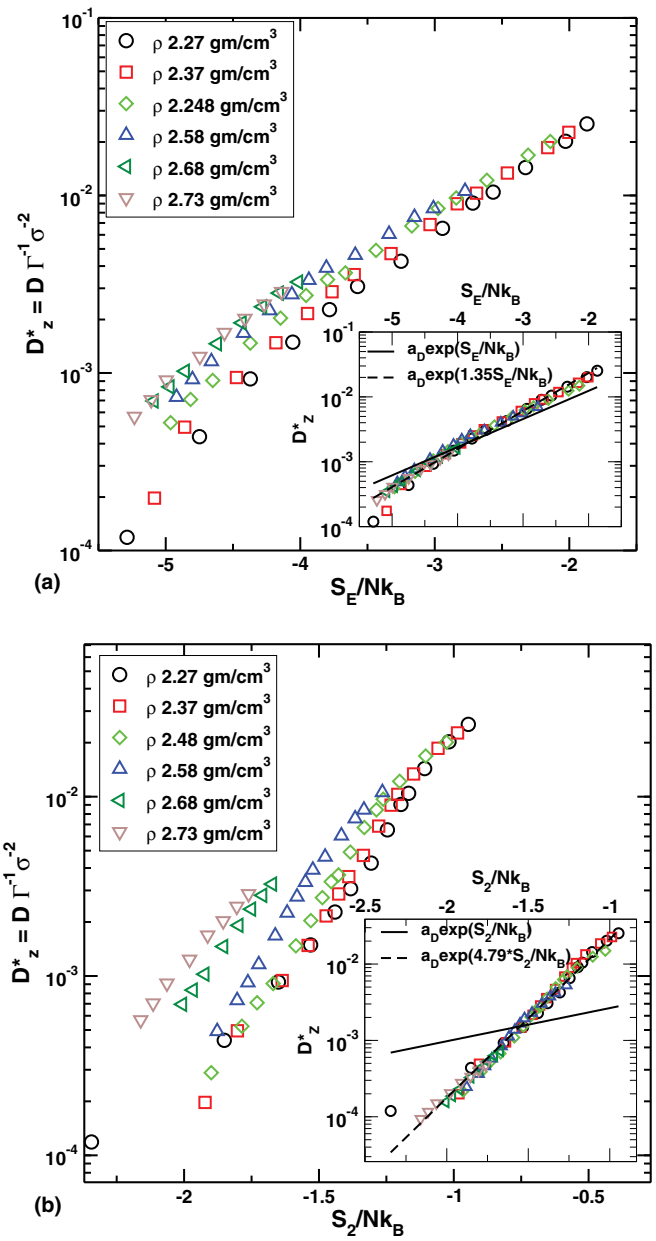

FIG. 18. Dzugutov scaling: The reduced diffusion coefficient against the excess entropy for different isochores. (Inset) The isochores collapse when the diffusivity curves are shifted by a constant term (by hand) and fit to a single function with a fit coefficient of 1.35 (using S_E) and 4.79 (using S_2).

non-anomalous branch of isotherms (where the excess entropy decreases with density). We note that liquid silicon failing to follow the Dzugutov scaling law has been reported in two of the previous studies[14,44] using the pair correlation entropy S_2 and we find similar results with S_2. When we use the total excess entropy S_E we find a substantial improvement in which the Dzugutov scaling exponent is around 1.24, in the non-anomalous branch. The collision frequency, which goes as an input into the Dzugutov scaling relation, is obtained from the first peak of radial distribution function, which is an over-simplification in case of liquid silicon. At a given state point we have computed the radial distribution function explicitly for tetrahedrally coordinated particles and 5-coordinated particles and find an evident difference in the amplitude and peak position of g(r). We also find that the mobility of a tetrahedrally coordinated particle differs from particles having more than four neighbours. These observations suggest a need for better estimation of collision frequency which we do not attempt to do in this work.

For the purpose of understanding the relation between excess entropy and diffusion coefficient, we use arithmetic average of the exponents (obtained from the non-anomalous branch) and verify the criterion to predict onset of diffusion anomaly. The average exponent we get, using the pair correlation entropy, is $b_D = 4.10$ and using the total excess entropy is $b_D = 1.08$ (in the Rosenfeld scaling relation) and 1.24 (in the Dzugutov scaling relation). We use the criterion obtained from the Rosenfeld relation ($\partial s_E/\partial \ln(\rho)|_T > 1/(3|b_D|)$) and the Dzugutov relation ($\partial s_E/\partial \ln(\rho)|_T > -1$) to extract the

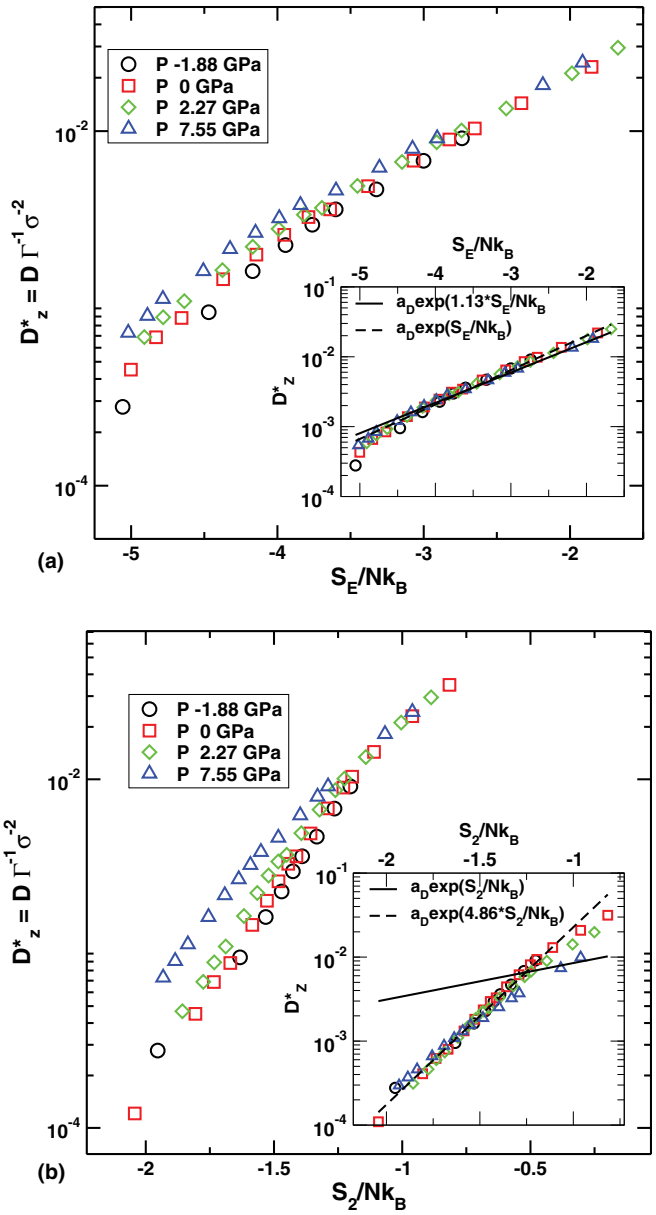

FIG. 19. Dzugutov scaling: The reduced diffusion coefficient against the excess entropy for different isobars. (Inset) The isobars collapse when the diffusivity curves are shifted by a constant term (by hand) and fit to a single function with a fit coefficient of 1.13 (using S_E) and 4.86 (using S_2).

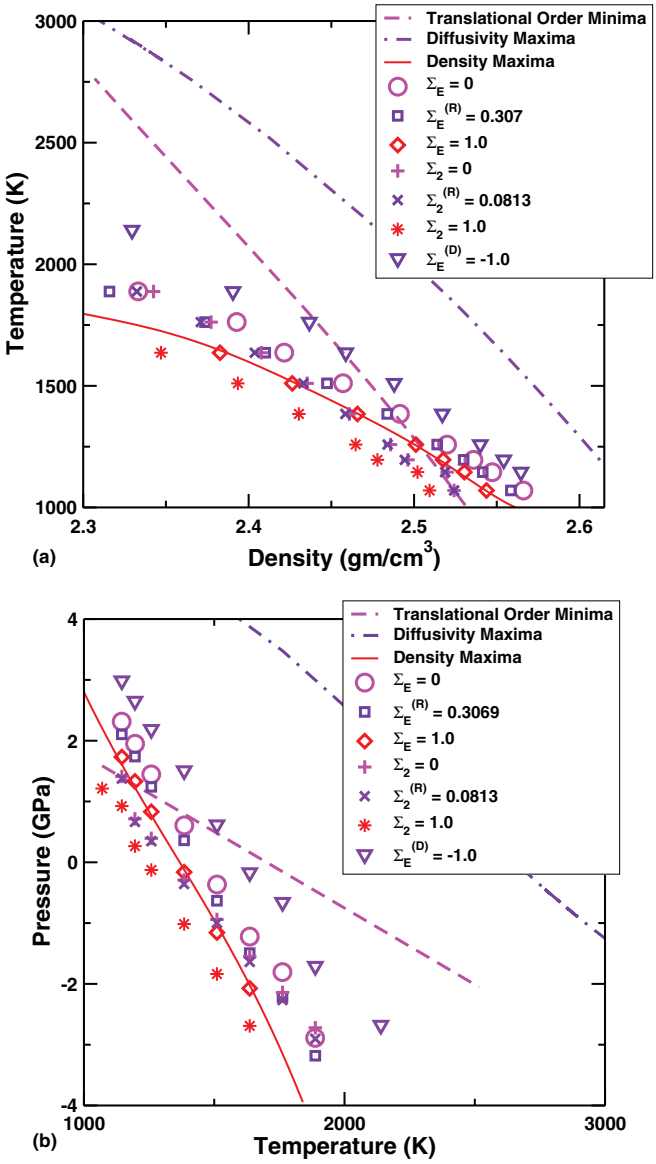

FIG. 20. Phase diagram of liquid silicon in (a) (T, ρ) plane and (b) (P, T) plane showing the loci of density maxima, translational order minima, and diffusivity maxima along with the estimates of these loci obtained from excess entropy.

temperature and density (and pressure from the equation of state) corresponding to the onset of diffusivity anomalies. In Fig. 20 we show the phase diagram along with the loci of anomalies obtained using the excess entropy. The excess entropy predicts the onset of density anomaly but not the diffusivity and structural anomalies. The estimates from excess entropy severely underestimate the value of the onset temperature and density (pressure) and are also unable to capture the overall slopes of the loci.

TABLE II. The scaling coefficients obtained along different paths in the phase diagram. The superscripts R and D indicate Rosenfeld scaling and Dzugutov scaling. Isotherm (n) implies the normal branch and isotherm (a) implies the anomalous branch of the scaling curve.

	$S_E^{(R)}$	$S_2^{(R)}$	$S_E^{(D)}$	$S_2^{(D)}$
Isochore	1.07	4.08	1.35	4.79
Isobar	1.02	4.38	1.13	4.86
Isotherm(n)	1.17	3.84	1.25	4.53
Isotherm(a)	1.23	2.67	1.37	3.10

IV. DISCUSSION

Understanding the relation between the structural ordering, dynamics, and thermodynamics is of fundamental importance. In systems like water, silica, and others systems which show water-like anomalies these relations have been studied in the context of understanding anomalies. In this work we have looked at two important aspects related to water-like anomalies in the system of liquid silicon, modeled by the Stillinger-Weber potential. The first aspect is related to the nesting of regions of different anomalies in liquid silicon. The thermodynamic anomaly related to the density has been

previously reported in the work of Vasisht *et al.*[13] In this work we trace the boundaries of the regions of diffusivity anomaly and structural anomaly. Following previous work on water[9] and silica[10] we have performed structural analysis using the translational and tetrahedrality order parameters. In silicon we indeed find the onset of structural anomaly (defined by the minima in the translation order parameter), but not the end of the structurally anomalous region (defined by the maxima in tetrahedrality order) before reaching the liquid-gas spinodal. The order of appearance is similar to that of silica,[10] wherein the region of diffusivity anomaly includes the region of structural anomaly, which in turn encompasses the region of density anomaly. At low temperatures, the regions of thermodynamic anomaly and structural anomaly reverse in order. In our analysis of translational order at very high temperatures we observe that the average t_{trans} can go through a minimum beyond the liquid-gas critical point. We need to investigate this feature further, since it raises questions about the definition of the structurally anomalous region. In this work we also analyse the local orientational order parameter q_3 and find that at high densities and temperatures, q_3 is a better order parameter to use. We also find that the feature of structural order parameters, in the anomalous region, being uniquely related to each other weakens (a feature observed in silica[10]) and hence this feature clearly depends on how one measures the orientational order.

The second aspect of this work is related to excess entropy and its relation with the anomalies. We compute the total excess entropy (using the method of thermodynamic integration) and compare it with the pair correlation entropy. The estimates of s_2 are smaller in magnitude than s_E as we are ignoring the contribution of higher order correlations but the profile as a function of density and pressure is quite similar. Since the orientational ordering is lower at high densities at low temperatures, and at low densities at high temperatures (as is clear at least using q_{tetra}), we expect the proportionality between the two measures of excess entropy to be better at these state points, and the data indeed support the expectation. In this context we have tested the Rosenfeld scaling relation and also the Dzugutov scaling relation. Using the total excess entropy, we find that Dzugutov scaling works reasonably well, and better than the one obtained using the pair correlation entropy. The Rosenfeld relation also works reasonably, in particular at high temperatures, but involves a fit coefficient that has considerable variation as a function of density.

ACKNOWLEDGMENTS

We acknowledge the use of the computational facilities at TUS-CMS (CCMS), Jawaharlal Nehru Centre for Advanced Scientific Research, Bengaluru, India. We thank Charusita Chakravarty and Murari Singh for useful discussions.

APPENDIX: EXCESS ENTROPY COMPUTATION

1. Excess entropy and other excess quantities

Under constant volume and temperature (NVT) conditions, the excess entropy S_E of a system is naturally defined as the total entropy of the system minus the entropy of the monatomic ideal gas at the same density and temperature as the system. However, the present work is mainly done under constant pressure and temperature (NPT) conditions. Since a liquid can be at zero or negative pressures where the ideal gas state is not defined, the above definition is a sensible choice even under NPT conditions. Thus, the excess entropy computed in our work at a given pressure and temperature is defined as

$$\begin{aligned} S_E(P,T) &\equiv S_E(\rho(P,T),T) \\ &= S(\rho(P,T),T) - S_{\mathrm{id}}(\rho(P,T),T), \end{aligned} \tag{A1}$$

where S is the total entropy of the system (SW model), S_{id} is the entropy of the ideal gas, and ρ is the density of the system corresponding to the pressure P and temperature T.

In analogy with the above definition of excess entropy, we also define the excess Helmholtz free energy F_E, the excess Gibbs free energy G_E, and the excess enthalpy H_E for later reference:

$$\begin{aligned} F_E(P,T) &\equiv F_E(\rho(P,T),T) \\ &= F(\rho(P,T),T) - F_{\mathrm{id}}(\rho(P,T),T) \\ &= U(P,T) - TS_E(P,T), \end{aligned} \tag{A2}$$

$$\begin{aligned} G_E(P,T) &\equiv G_E(\rho(P,T),T) \\ &= G(\rho(P,T),T) - G_{\mathrm{id}}(\rho(P,T),T) \\ &= U(P,T) + PV - Nk_BT - TS_E(P,T), \end{aligned} \tag{A3}$$

$$\begin{aligned} H_E(P,T) &\equiv H_E(\rho(P,T),T) \\ &= H(\rho(P,T),T) - H_{\mathrm{id}}(\rho(P,T),T) \\ &= U(P,T) + PV - Nk_BT, \end{aligned} \tag{A4}$$

where $F = E - TS$ is the total Helmholtz free energy, $G = E + PV - TS$ is the total Gibbs free energy, $H = E + PV$ is the total enthalpy of the system, and $E = K + U$ is the total energy of the system with K denoting the kinetic energy and U standing for the potential energy. Symbols with the suffix "id" denotes the corresponding quantities for the ideal gas.

2. Outline of thermodynamic integration employed

To compute the entropy of the system we use the method of thermodynamic integration, in which an appropriate derivative of entropy is integrated along a reversible path from a reference state of known entropy to the target state point. The integral gives the difference in entropy between the target and the reference state points. By adding the value of the entropy at the reference state point to the integral, the entropy at the target state point is computed. The path of the thermodynamic integration in the phase diagram was chosen such that no first-order transition was encountered. For the SW model at $\lambda = 21$, the path is shown in Fig. 21. However, for the sake of completeness we also discuss the entropy calculation for the modified SW model at a general λ values. The brief outline of the method is given below and further details are discussed separately in Subsection A 3 of the Appendix.

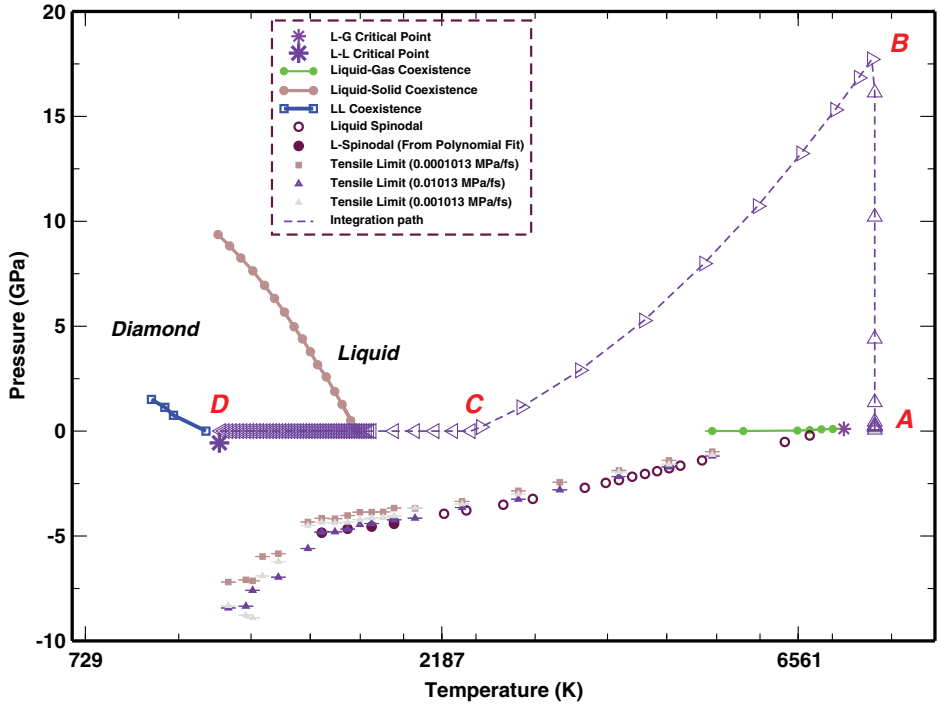

FIG. 21. The path of the thermodynamic integration is shown in the P-T phase diagram for silicon.

The reference state point: We choose $T = 8308\,K$ and $P = 0\,GPa$ (point **A** in Fig. 21 which is above the liquid-gas critical point) as the reference state point where the SW model ($\lambda = 21$) is assumed to behave as an ideal gas, i.e., the total entropy of the system is given by that of the ideal gas and hence the excess entropy is zero.

Step 1: Excess entropy at a reference T at zero pressure: From the reference state point, the excess entropy at a temperature $T = 2391$ K and at $P = 0$ GPa (point **C** in Fig. 21) is obtained by integrating appropriate derivatives computed from the equation of state and the potential energy data. The density of SW model at point **C** is $\rho_C = 2.41$ gm/cm^3. In order to avoid the liquid-gas critical point, we first perform the thermodynamic integration along the $T = 8308$ K isotherm **AB**, going from point **A** to a point **B** with density $\rho_B = \rho_C = 2.41$ gm/cm^3 and then from point **B** to point **C** along the isochore **BC**.

Step 2: Excess entropy at other T along zero pressure isobar: From the excess entropy at $T = 2391$ K and at $P = 0$ GPa, the excess entropy at other temperatures along the $P = 0$ GPa isobar (**CD** in Fig. 21) is obtained by integrating appropriate derivatives of entropy computed from the specific heat data.

Step 3a: Excess entropy to non-zero pressures along different isotherms: Finally, the excess entropy at a non-zero pressure and a given temperature is computed by starting from zero pressure value of the excess entropy obtained in the previous step and integrating the appropriate derivatives obtained from the equation of state data along an isotherm.

Step 3b: Excess entropy to other λ values at constant P, T: To compute the excess entropy at a general λ value, we modify the interaction potential by tuning the parameter λ at constant pressure and temperature to go from the SW model at $\lambda = 21$ to a modified SW model at a general λ. We choose a temperature T on the $P = 0$ GPa isobar of the SW model ($\lambda = 21$) as the reference state point where entropy is computed using the procedure described above. Then the appropriate derivative of entropy with respect to λ was integrated from $\lambda = 21$ to a general λ value at constant $P = 0$ GPa, T to compute the difference in entropy. Next the reference entropy value at $P = 0$ GPa, T, $\lambda = 21$ was added to obtain the entropy at a general λ value at $P = 0$ GPa, T.

Step 4: Excess entropy at other T along zero pressure isobar at a general λ: From the excess entropy at $T = T_0$ and at $P = 0$ GPa, the excess entropy at other temperatures along the $P = 0$ GPa at a general λ is obtained by integrating appropriate derivatives of entropy computed from the specific heat data as in Step 2.

3. Computational details of thermodynamic integration

Step 1: Excess entropy at a reference T at zero pressure: Along the isotherm **AB** and the isochore **BC**, the derivatives of the excess Helmholtz free energy F_E can be directly computed from the excess pressure P_E and potential energy U, respectively,

$$\left[\frac{\partial F_E}{\partial \rho}\right]_{T,N} = \frac{P_E}{\rho^2} \equiv \frac{P - \rho T}{\rho^2} \quad \text{along AB},$$
$$\left[\frac{\partial (F_E/T)}{\partial T}\right]_{\rho,N} = \left(\frac{-U}{T^2}\right) \quad \text{along BC}. \tag{A5}$$

These identities were used to compute the change in excess Helmholtz free energy from point **A** to point **C**. Since the SW model is assumed to behave as an ideal gas at the point **A**, the excess Helmholtz free energy at point **A** is zero. Hence the excess Helmholtz free energy at point **C** can be computed using Eq. (A5). Finally, the excess entropy at point **C** is obtained

from the excess Helmholtz free energy using the definitions (A1) and (A2). The procedure is summarized below:

$$\begin{aligned} S_E(P=0,T_C) &\equiv S_E(\rho_C,T_C) \\ &= \frac{U(\rho_C,T_C)}{T_C} - \frac{F_E(\rho_C,T_C)}{T_C}, \\ \frac{F_E(\rho_C,T_C)}{T_C} &= \frac{F_E(\rho_B,T_B)}{T_B} + \int_{T_B}^{T_C} dT \left(\frac{-U}{T^2}\right), \\ F_E(\rho_B,T_B) &= F_E(\rho_A,T_A) + \int_{\rho_A}^{\rho_B} d\rho \frac{P_E}{\rho^2}, \\ F_E(\rho_A,T_A) &= 0, \end{aligned} \tag{A6}$$

where $T_A = T_B = 8308\,\text{K}$, $T_C = 2391\,\text{K}$, $\rho_A \equiv \rho(0, T_A)$ is the density of the SW model at $P = 0\,\text{GPa}$, $T = 8308\,\text{K}$.

Step 2: Excess entropy at other T along zero pressure isobar: Along an isobar, the derivative of the total entropy can be obtained from the specific heat C_P using the identity

$$\left[\frac{\partial S}{\partial T}\right]_{P,N} = \frac{C_P}{T}. \tag{A7}$$

Using the definition, Eq. (A1), and the identity, Eq. (A7), the excess entropy at a temperature T along $P = 0\,\text{GPa}$ isobar is given by

$$\begin{aligned} S_E(0,T) &= S_E(0,T_C) + \Delta S_E(0,T) \\ &= S_E(0,T_C) + \Delta S(0,T) - \Delta S_{id}(0,T) \\ &= S_E(0,T_C) + \int_{T_C}^{T} \frac{C_P(T')}{T'} dT' \\ &\quad - \left[\frac{3Nk_B}{2}\ln\left(\frac{T}{T_C}\right) - Nk_B \ln\left(\frac{\rho(0,T)}{\rho_C}\right)\right], \end{aligned} \tag{A8}$$

where $\Delta S_E(0, T)$, $\Delta S(0, T) \equiv S(0, T) - S(0, T_C)$, and $\Delta S_{id}(0, T) \equiv S_{id}(\rho(0, T), T) - S_{id}(\rho_C, T_C)$ are the changes in the excess, the total, and the ideal gas entropy along the $P = 0\,\text{GPa}$ isobar from temperature T_C to T, respectively. The ideal gas entropy at the SW liquid density $\rho(0, T)$ on the isobar $P = 0\,\text{GPa}$ is given by the Sackur-Tetrode formula: $\frac{S_{id}}{Nk_B} = \frac{3}{2} - (3\ln(\Lambda) + \ln(\rho) - 1)$, where $\Lambda = (\frac{2\pi\hbar^2}{mk_BT})^{1/2}$.

Now, we discuss ways to rewrite Eq. (A8) to compare with recent works[37,38] in literature where the excess entropy in SW model under constant pressure condition was computed. First, the full specific heat C_P can be resolved into a kinetic or momentum space contribution C_P^K and a "configuration space" contribution C_P^C as

$$\begin{aligned} C_P &= \frac{\langle H^2\rangle - \langle H\rangle^2}{k_BT^2} \\ &= \frac{[\langle K^2\rangle - \langle K\rangle^2]}{k_BT^2} + \frac{[\langle H_C^2\rangle - \langle H_C\rangle^2]}{k_BT^2} \\ &\equiv C_P^K + C_P^C \\ &= \frac{3}{2}Nk_B + C_P^C, \end{aligned} \tag{A9}$$

where $C_P^K \equiv \frac{\langle K^2\rangle - \langle K\rangle^2}{k_BT^2}$, $C_P^C \equiv \frac{\langle H_C^2\rangle - \langle H_C\rangle^2}{k_BT^2}$ and H_C is the "configurational" part of the enthalpy defined as $H = K + U + PV \equiv K + H_C$. Next, as a consequence of definition (A1), the infinitesimal reversible change in excess entropy dS_E along an isobar from state point (N, P, T) to $(N, P, T + dT)$ is given by

$$\begin{aligned} TdS &= C_p dT, \\ TdS_{id} &= dE_{id} + P_{id}dV \\ &= \frac{3}{2}Nk_B dT + Nk_BT\frac{dV}{V}, \\ TdS_E &= TdS - TdS_{id} \\ &= \left(C_p - \frac{3}{2}Nk_B\right)dT - Nk_BT\frac{dV}{V}, \\ dS_E &= \frac{C_P^C}{T}dT + Nk_B\frac{d\rho}{\rho}, \end{aligned} \tag{A10}$$

where $E_{id} = \frac{3}{2}Nk_BT$ is the energy and $P_{id} = \frac{Nk_BT}{V}$ is the pressure of an ideal gas at the same density and temperature as the SW system. We note that P_{id} is in general different from the SW pressure P because the SW model and the ideal gas follow different equations of state. Hence, using Eq. (A10), Eq. (A8) can be rewritten as

$$\begin{aligned} S_E(0,T) &= S_E(0,T_C) \\ &\quad + \int_{T_C}^{T} \frac{C_P^C(T')}{T'}dT' + Nk_B\ln\left(\frac{\rho(0,T)}{\rho_C}\right), \\ C_P^C &= C_P - \frac{3}{2}Nk_B \\ &= \frac{\langle H_C^2\rangle - \langle H_C\rangle^2}{k_BT^2} \\ &= \frac{\langle H_E^2\rangle - \langle H_E\rangle^2}{k_BT^2}. \end{aligned} \tag{A11}$$

The last relation holds because at constant (N, P, T) condition $H_C = H_E - Nk_BT$ differs from H_E only by a constant. Next, in analogy to the identity $C_P = (\frac{dH}{dT})_P$ for the full specific heat, we define an excess specific heat $C_P^E \equiv (\frac{dH_E}{dT})_P$. From the definition, Eq. (A4), the infinitesimal reversible change in excess enthalpy along an isobar from state point (N, P, T) to $(N, P, T + dT)$ will be

$$\begin{aligned} dH &= C_p dT, \\ dH_{id} &= \frac{5}{2}Nk_B dT, \\ dH_E &= \left(C_p - \frac{5}{2}Nk_B\right)dT \\ &\equiv C_p^E dT, \end{aligned} \tag{A12}$$

where $H_{id} = E_{id} + P_{id}V = \frac{5}{2}Nk_BT$ is the enthalpy of the ideal gas at the same density and temperature as the SW system. Hence, using Eqs. (A10) and (A12), Eq. (A8) can be

rewritten as

$$dS_E = \frac{C_P^E}{T}dT + Nk_B\frac{dT}{T} + Nk_B\frac{d\rho}{\rho},$$

$$S_E(0,T) = S_E(0,T_C) + \int_{T_C}^{T}\frac{C_P^E(T')}{T'}dT' + Nk_B\left(\ln\frac{T}{T_C} + \ln\frac{\rho(0,T)}{\rho_C}\right),$$

$$C_P^E = C_P - \frac{5}{2}Nk_B = \left(\frac{dH_E}{dT}\right)_P. \quad \text{(A13)}$$

We note that in Ref. 37, the excess entropy under constant pressure condition was defined differently such that the ideal gas was considered to be at a constant pressure. The procedure used in Ref. 37 amounted to omitting the term $Nk_B \ln\frac{\rho T}{\rho_C T_C}$ from Eq. (A13).

Step 3a: Excess entropy to non-zero pressures along different isotherms: Along an isotherm, the derivative of the Gibbs free energy can be directly computed from the identity

$$\left[\frac{\partial G}{\partial P}\right]_{T,N} = V. \quad \text{(A14)}$$

The above identity was used to compute the change in the total Gibbs free energy from $P = 0$ GPa to a non-zero P along an isotherm and hence the excess Gibbs free energy G_E at a non-zero pressure. Then the excess entropy S_E at a non-zero pressure P was computed from G_E using Eq. (A3). The procedure is summarized below:

$$S_E(P,T) = \frac{U(P,T) + PV - Nk_BT}{T} - \frac{G_E(P,T)}{T},$$

$$G_E(P,T) = G_E(0,T) + \Delta G_E(P,T) = G_E(0,T) + \Delta G(P,T) - \Delta G_{id}(P,T) = G_E(0,T) + \int_0^P V(P',T)dP' - Nk_BT\ln\left(\frac{\rho(P,T)}{\rho(0,T)}\right),$$

$$G_E(0,T) = U(0,T) - Nk_BT - TS_E(0,T), \quad \text{(A15)}$$

where $\Delta G_E(P,T)$, $\Delta G(P,T) \equiv G(P,T) - G(0,T)$, and $\Delta G_{id}(P,T) \equiv G_{id}(\rho(P,T),T) - G_{id}(\rho(0,T),T)$ are the changes in the excess, the total, and the ideal gas Gibbs free energies, respectively, along an isotherm T from $P = 0$ GPa to a non-zero P. The ideal gas Gibbs free energy at the SW system density $\rho(P,T)$ is given by $G_{id}(\rho(P,T),T) = Nk_BT\ln(\rho\Lambda^3)$.

Step 3b: Excess entropy to other λ values at constant P, T: At constant pressure and temperature, the derivative of the Gibbs free energy $G(\lambda)$ with respect to λ can be directly computed using the following identity:

$$\frac{\partial G}{\partial\lambda} = \left\langle\frac{\partial U}{\partial\lambda}\right\rangle_\lambda \text{ (ensemble average at fixed } \lambda) = \left\langle\frac{\partial(U_2 + \lambda U_3)}{\partial\lambda}\right\rangle_\lambda = \langle U_3\rangle_\lambda, \quad \text{(A16)}$$

where U is the total SW potential energy, U_2 is the part of potential independent of λ, and λU_3 is the λ-dependent part of U. The above identity was used to compute the change in the total Gibbs free energy from $\lambda = 21$ to a general λ at $P = 0$ GPa, T and hence the excess Gibbs free energy $G_E(\lambda)$ at a general λ. Then the excess entropy at a general λ at $P = 0$ GPa, T is computed from using Eq. (A3). The procedure is summarized below:

$$S_E(\lambda,P,T) = S(\lambda,P,T) - S_{id}(\rho(\lambda,P,T),T) = \frac{U(\lambda,P,T) + PV(\lambda,P,T) - Nk_BT - G_E(\lambda,P,T)}{T},$$

$$G_E(\lambda,P,T) = G_E(21,P,T) + \Delta G_E(\lambda) = G_E(21,P,T) + \Delta G(\lambda) - \Delta G_{id}(\lambda) = G_E(21,P,T) + \int_{21}^{\lambda}\langle U_3\rangle_{\lambda'}d\lambda' - Nk_BT\ln\frac{\rho(\lambda,P,T)}{\rho(21,P,T)},$$

$$G_E(21,P,T) = U(21,P,T) + PV(21,P,T) - Nk_BT - TS_E(21,P,T), \quad \text{(A17)}$$

where $S_{id}(\rho(\lambda,P,T),T) = \frac{E_{id} + P_{id}V(\lambda) - G_{id}(\lambda)}{T}$ is the ideal gas entropy at a general λ, $\Delta G(\lambda) \equiv G(\lambda,P,T) - G(21,P,T)$ is the change in the system Gibbs free energy, and $\Delta G_{id}(\lambda) \equiv G_{id}(\rho(\lambda,P,T),T) - G_{id}(\rho(21,P,T),T)$ is the change in the Gibbs free energy of the ideal gas from $\lambda = 21$ to a general λ at fixed pressure and temperature.

Combining all terms and setting $P = 0$, Eq. (A17) can be simplified to

$$S_E(\lambda,0,T) = S_E(21,0,T) + \left[\frac{\Delta U(\lambda) - \int_{21}^{\lambda}\langle U_3\rangle_{\lambda'}d\lambda'}{T}\right] + Nk_B\ln\frac{\rho(\lambda)}{\rho(21)} \equiv S_E(21,0,T) + \Delta S(\lambda) - \Delta S_{id}(\lambda), \quad \text{(A18)}$$

where $\Delta S(\lambda) \equiv S(\lambda,0,T) - S(21,0,T)$ and $\Delta S_{id}(\lambda)$ are the changes in the system entropy and ideal gas entropy, respectively, from $\lambda = 21$ to a general λ at $P = 0$ GPa and a fixed T. Note that the ideal gas part of free energy and entropy depends on λ because the density ρ of the SW liquid at constant temperature and pressure is a function of λ.

Step 4: Excess entropy at other T along zero pressure isobar at a general λ: The computational details of this step are already discussed in step 2 in Subsection A 3 of the Appendix. From the excess entropy at a general λ at $P = 0$ GPa, T, the excess entropy at other temperatures at $P = 0$ GPa is computed using either Eq. (A8), (A11), or (A13) where the specific heats C_P, C_P^C, C_P^E and the density ρ are now functions of λ.

[1] M. Chaplin, *Water structure and science*, see http://www.lsbu.ac.uk/water/anmlies.html.
[2] P. G. Debenedetti, *Metastable Liquids: Concepts and Principles* (Princeton University Press, 1996).
[3] O. Mishima and H. E. Stanley, Nature (London) **396**, 329 (1998).
[4] I. Brovchenko and A. Oleinikova, ChemPhysChem **9**, 2660 (2008).
[5] R. J. Speedy and C. A. Angell, J. Chem. Phys. **65**, 851 (1976).
[6] P. H. Poole, F. Sciortino, U. Essmann, and H. E. Stanley, Nature (London) **360**, 324 (1992).
[7] S. Sastry, P. G. Debenedetti, F. Sciortino, and H. E. Stanley, Phys. Rev. E **53**, 6144 (1996).
[8] C. A. Angell, Science **319**, 582 (2008).
[9] J. R. Errington and P. G. Debenedetti, Nature (London) **409**, 318 (2001).
[10] M. S. Shell, P. G. Debenedetti, and A. Z. Panagiotopoulos, Phys. Rev. E **66**, 011202 (2002).
[11] F. Sciortino, A. Geiger, and H. E. Stanley, Nature (London) **354**, 218 (1991).
[12] T. Morishita, Phys. Rev. E **72**, 021201 (2005).
[13] V. V. Vasisht, S. Saw, and S. Sastry, Nat. Phys. **7**, 549 (2011).
[14] G. X. Li, C. S. Liu, and Z. G. Zhu, J. Non-Cryst. Solids **351**, 946 (2005).
[15] J. Mittal, J. R. Errington, and T. M. Truskett, J. Chem. Phys. **125**, 076102 (2006).
[16] R. Sharma, S. N. Chakraborty, and C. Chakravarty, J. Chem. Phys. **125**, 204501 (2006).
[17] Y. D. Fomin, E. N. Tsiok, and V. N. Ryzhov, Phys. Rev. E **87**, 042122 (2013).
[18] Z. Yan, S. V. Buldyrev, N. Giovambattista, and H. E. Stanley, Phys. Rev. Lett. **95**, 130604 (2005).
[19] L. Xu, S. V. Buldyrev, C. A. Angell, and H. E. Stanley, Phys. Rev. E **74**, 031108 (2006).
[20] W. P. Krekelberg, J. Mittal, V. Ganesan, and T. M. Truskett, J. Chem. Phys. **127**, 044502 (2007).
[21] A. B. de Oliveira, G. Franzese, P. A. Netz, and M. C. Barbosa, J. Chem. Phys. **128**, 064901 (2008).
[22] A. B. de Oliveira, P. A. Netz, and M. C. Barbosa, Europhys. Lett. **85**, 36001 (2009).
[23] B. S. Jabes, M. Agarwal, and C. Chakravarty, J. Chem. Phys. **132**, 234507 (2010).
[24] B. S. Jabes, D. Nayar, D. Dhabal, V. Molinero, and C. Chakravarty, J. Phys.: Condens. Matter **24**, 284116 (2012).
[25] W. Hujo, B. S. Jabes, V. K. Rana, C. Chakravarty, and V. Molinero, J. Stat. Phys. **145**, 293 (2011).
[26] D. Nayar, M. Agarwal, and C. Chakravarty, J. Chem. Theory Comput. **7**, 3354 (2011).
[27] M. Agarwal, P. A. Mohammad, and C. Chakravarty, J. Phys. Chem. B **115**, 6935 (2011).
[28] J. R. Errington, T. M. Truskett, and J. Mittal, J. Chem. Phys. **125**, 244502 (2006).
[29] R. Sharma, A. Mudi, and C. Chakravarty, J. Chem. Phys. **125**, 044705 (2006).
[30] R. Sharma, M. Agarwal, and C. Chakravarty, Mol. Phys. **106**, 1925 (2008).
[31] F. H. Stillinger and T. A. Weber, Phys. Rev. B **31**, 5262 (1985).
[32] V. V. Vasisht and S. Sastry, *Liquid Polymorphism* (John Wiley & Sons, Inc., 2013), p. 463.
[33] P. H. Poole, I. Saika-Voivod, and F. Sciortino, J. Phys.: Condens. Matter **17**, L431 (2005).
[34] I. Saika-Voivod, F. Sciortino, and P. H. Poole, Phys. Rev. E **63**, 011202 (2000).
[35] T. M. Truskett, S. Torquato, and P. G. Debenedetti, Phys. Rev. E **62**, 993 (2000).
[36] P. J. Steinhardt, D. R. Nelson, and M. Ronchetti, Phys. Rev. B **28**, 784 (1983).
[37] S. Sengupta, V. V. Vasisht, and S. Sastry, J. Chem. Phys. **140**, 044503 (2014).
[38] M. Singh, D. Dhabal, A. H. Nguyen, V. Molinero, and C. Chakravarty, Phys. Rev. Lett. **112**, 147801 (2014).
[39] R. E. Nettleton and M. S. Green, J. Chem. Phys. **29**, 1365 (1958).
[40] A. Baranyai and D. J. Evans, Phys. Rev. A **40**, 3817 (1989).
[41] R. M. Lynden-Bell and P. G. Debenedetti, J. Phys. Chem. B **109**, 6527 (2005).
[42] Y. Rosenfeld, J. Phys.: Condens. Matter **11**, 5415 (1999).
[43] M. Dzugutov, Nature (London) **381**, 137 (1996).
[44] J. J. Hoyt, M. Asta, and B. Sadigh, Phys. Rev. Lett. **85**, 594 (2000).
[45] M. Agarwal, M. Singh, R. Sharma, P. A. Mohammad, and C. Chakravarty, J. Phys. Chem. B **114**, 6995 (2010).